On the third-order nonlinear optical responses of cis and trans stilbenes - a quantum chemistry investigation

Kaka, Komlanvi Sèvi; Castet, Frédéric; Champagne, Benoît

Published in:
PCCP : Physical Chemistry Chemical Physics

DOI:
10.1039/d4cp00522h

Publication date:
2024

PCCP
Physical Chemistry Chemical Physics

Accepted Manuscript

This article can be cited before page numbers have been issued, to do this please use: K. S. KAKA, F. Castet and B. R. Champagne, *Phys. Chem. Chem. Phys.*, 2024, DOI: 10.1039/D4CP00522H.

ROYAL SOCIETY OF CHEMISTRY

rsc.li/pccp

On the third-order nonlinear optical responses of *cis* and *trans* stilbene – a quantum chemistry investigation†

View Article Online
DOI: 10.1039/D4CP00522H

Komlanvi Sèvi Kaka,[‡] Frédéric Castet,[£] and Benoît Champagne[‡,*]

[‡] *Theoretical Chemistry Laboratory, Unit of Theoretical and Structural Physical Chemistry, NISM (Namur Institute of Structured Matter), University of Namur (UNamur), B-5000 Namur, Belgium*

[£] *University of Bordeaux, CNRS, Bordeaux INP, ISM, UMR 5255, F-33405 Cedex Talence, France.*

e-mail: benoit.champagne@unamur.be

† **Electronic supplementary information (ESI) available**: complements on experimental techniques to measure the second hyperpolarizabilities; structures and energies of the *trans* and *cis* stilbenes; numerical aspects on the calculation of second hyperpolarizabilities; basis set and electron correlation effects; impact of the choice of exchange-correlation functional; solvent effects, frequency dispersion and vibrational second hyperpolarizability.

ABSTRACT.

The second hyperpolarizabilities (γ) of the stilbene molecular switch in its *trans* and *cis* forms have been calculated using quantum chemistry methods to address their third-order nonlinear optical contrasts, to assess the reliability of lower-cost DFT methods, and to make comparisons with experiments. First, the reference CCSD(T) method shows that *trans*-stilbene presents a $\gamma_{//}$ value twice larger than its *cis* isomer (its γ_{THS} value is 2.7 times larger). Among more cost-effective methods, reliable results are obtained at the MP2 as well as with DFT, provided the CAM-B3LYP or ωB97X-D XCFs are employed. Supplementary DFT calculations have investigated the relationships between the accuracy of the exchange-correlation functionals, the fulfillment of Koopmans' theorem, and the delocalization error, and they demonstrated that satisfying Koopmans' theorem is not the condition for the best accuracy but that functionals with small delocalization errors are generally efficient. Using the selected CAM-B3LYP, large γ enhancements by about 70% (*trans*-stilbene) and 50% (*cis*-stilbene) have been evidenced when accounting for solvent effect using an implicit solvation model (IEFPCM), even for apolar solvents. Then, the frequency dispersion of the γ responses has been described using Bishop polynomial expansions, allowing comparisons with a broad set of experimental data. To a certain extent, no systematic agreement between the calculations and the measured values was found. On the one hand, the agreement is satisfactory for the $\gamma(-\omega;\ \omega,-\omega,\omega)$ quantities, provided the dominant vibrational contribution is taken into account. On the other hand, the agreement is poor for the $\gamma(-2\omega;\omega,\omega,0)$ and $\gamma(-3\omega;\ \omega,\omega,\omega)$ quantities, while some inconsistencies between experimental values are also highlighted.

DOI: 10.1039/D4CP00522H

I. Introduction

The interaction of an intense laser field with matter produces a number of phenomena of interest in the field of nonlinear optics.[1] Third-order nonlinear optical (NLO) responses are of prime interest because materials with large effects could foster the development of advanced technologies in optoelectronics and photonics.[2–4] One of the material classes under consideration for large and fast third-order nonlinearities are organic molecules, because of their low dielectric constant and fast electronic responses. Moreover, organic photochromic materials[5] have received extensive attention because they allow reversible switching of their electronic and optical properties, necessary for the development of optoelectronic and photonic technologies. Among the most significant photochromes, azobenzene, stilbene, and their derivatives undergo a uniquely clean and efficient photoisomerization, exhibiting thus a facile isomerization between their stable *cis* and *trans* geometries.[6,7] In the case of stilbene, the *cis* → *trans* conversion is driven by visible light radiation (400–500 nm) while the back reaction by ultraviolet light irradiation (340–400 nm) or heat.[8] Stilbene can also act as a third-order NLO molecule and several studies have experimentally characterized their responses.[9–14]

Efficient third-order NLO materials first require to be built from molecules that display large second hyperpolarizabilities (γ), the molecular property at the origin of these phenomena. Maximizing these γ responses has been carried out by resorting to experimental characterizations as well as by employing quantum chemistry (QC) calculations. Both have led to structure-property relationships, helpful to design new, more efficient compounds. Experimentally, recent papers have reported the measurement of the second hyperpolarizabilities using the third-harmonic scattering (THS) technique,[14,15] which has provided a new impetus in calculating these γ responses. In addition to THS, other experimental characterization techniques to determine γ encompass phase-conjugate interferometry (PCI),[11,16,17] degenerate four-wave mixing (DFWM), electric field-induced second harmonic generation (EFISHG),[18–20] and third harmonic generation (THG).[21,22] However, results obtained with different techniques can be difficult to compare. These difficulties originate from differences in laser frequencies and in solvents but also from the treatment of the output signals (e.g. using or not local field factor corrections), with differences in the calibration standards, and in the definition conventions.[23] They are compounded by the fact that the technical details of the experimental determinations are not systematically reported. This leads to broad distributions of values, even for prototypical NLO organic compounds,[24] making difficult the establishment of the structure-γ relationships. In parallel, QC calculations of these properties are complementary and can help rationalizing the experimental data, but accurate predictions require accounting for electron correlation and environment effects as well as for frequency dispersion, to quote a few effects.

Generally speaking, owing to the role of electron correlation, the uncorrelated Hartree-Fock (HF) method gives poor performance, while the correlated wavefunctions (WF) or density functional

View Article Online
DOI: 10.1039/D4CP00522H

theory (DFT) methods are recommended.[25–39] Unfortunately, there remain computational limitations in applying the former methods to large molecules, while employing DFT requires selecting reliable exchange-correlation functionals (XCFs).[40–48] In this context, we recently initiated a detailed investigation of the use of QC methods to predict and interpret the second hyperpolarizabilities of π-conjugated molecules, which can exhibit large responses. Our first study has dealt with *p*-nitroaniline (*p*NA), the prototypical push-pull π-conjugated molecule.[49] Using as reference the CCSD(T) method [coupled-cluster (CC) with singles and doubles as well as a perturbative treatment of triples], it was concluded that, among WF methods the second-order Møller-Plesset perturbation theory method (MP2) offers the best accuracy/cost ratio while at the DFT level, the best performance is achieved with double hybrid functionals.

There is however no guarantee that the same conclusions could be drawn when broadening the types of molecular systems. Accordingly, it is not surprising that benchmarking accuracy of various XCF has become an important task in computational chemistry.[49–53] So, in the present contribution, the performance of a broad range of QC methods for predicting and interpretating the second hyperpolarizability of the switchable *trans/cis*-stilbene compound (FIG. 1) is addressed in comparison to the reference CCSD(T) values. The frequency dispersion of γ is also characterized for different third-order NLO processes while solvent effects are described using the polarizable continuum model (PCM). These calculations then led to make comparisons with the recent THS measurements,[14] as well as prior experimental characterizations.

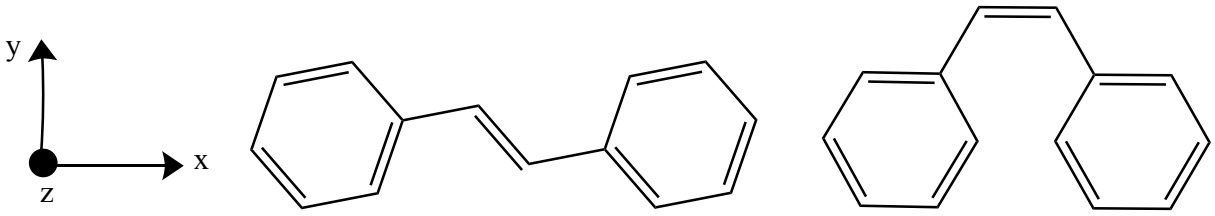

FIG. 1. Molecular structures of *trans*-stilbene (left) and *cis*-stilbene (right) in the Cartesian frame. The x-axis is defining the longitudinal direction (FIG S1).

II. Theoretical and computational aspects

II.A. The second hyperpolarizabilities and related experimental quantities

When external electric fields ($\vec{E}$) oscillating at frequencies ω_1, ω_2, ω_3 in the *i*, *j*, *k*, … directions are applied to a molecule, the induced dipole moment, $\Delta\mu_i(\vec{E})$, can be described via a Taylor expansion where the coefficients are the frequency-dependent polarizability, $\alpha_{ij}(-\omega_\sigma;\omega_1)$, the first and second hyperpolarizabilities, $\beta_{ijk}(-\omega_\sigma;\omega_1,\omega_2)$ and $\gamma_{ijkl}(-\omega_\sigma;\omega_1,\omega_2,\omega_3)$:

$$\Delta\mu_i(\vec{E}) = \sum_j^{x,y,z} \alpha_{ij}(-\omega_\sigma;\omega_1)E_j(\omega_1) + \frac{1}{2!}\sum_{jk}^{x,y,z} \beta_{ijk}(-\omega_\sigma;\omega_1,\omega_2)E_j(\omega_1)E_k(\omega_2) +$$

$$\frac{1}{3!}\sum_{jkl}^{x,y,z} \gamma_{ijkl}(-\omega_\sigma;\omega_1,\omega_2,\omega_3)E_j(\omega_1)E_k(\omega_2)E_l(\omega_3) + \cdots \quad (1)$$

where $\omega_\sigma = \sum_i^{1,2,\cdots}\omega_i$. The γ_{ijkl} components, which are the central quantities in the present study, form a rank-four tensor with a total of 81 elements. When the frequencies are far from electronic resonances (known as the Kleinman symmetry condition[54]), the number of independent elements reduces to 15. Considering Eq. (1), different third-NLO responses can be defined depending on the combination of static and dynamic incident electric fields. The most common ones are listed below, with more details in SI:

(i) The electric field induced second harmonic generation (EFISHG).[18–20,55] In this technique, optical electric field oscillating at frequency ω and a static electric field (which aligns the dipolar molecules) are simultaneously applied and the optical output at the second harmonic 2ω is measured. The SHG response reads:

$$\gamma_{EFISHG}(-2\omega;\omega,\omega,0) = \gamma_{//}(-2\omega;\omega,\omega,0) + \frac{\mu\beta_{//}(-2\omega;\omega,\omega)}{3kT} \quad (2)$$

$\beta_{//}$ is the vector component of the first hyperpolarizability tensor along the direction of the permanent molecular dipole moment, kT is the thermal energy of the medium where k is the Boltzmann constant and T is the absolute temperature. The scalar quantity $\gamma_{//}(-2\omega;\omega,\omega,0)$ is the isotropic average of the γ tensor. To disentangle the second- (if non negligible) and third-order contributions, measurements should be performed over a range of temperatures. Considering plane-polarized incident and emitted lights, the $\gamma_{//}$ quantity reads:

$$\gamma_{//}(-2\omega;\omega,\omega,0) = \frac{1}{15}\sum_{ij}^{x,y,z}\left(2\gamma_{iijj} + \gamma_{ijji}\right) \quad (3)$$

In the case of stilbene, the second-order contribution is negligible due to its molecular symmetry. The EFISHG response thus reduces to its third-order component.[10]

(ii) The degenerate four wave-mixing (DFWM).[9,56–58] In this measurement, three beams of frequency ω interact in the material and a fourth beam at the same frequency is produced. In this experiment, the quantity that can be extracted from the measurements reads:

$$\gamma_{DFWM}(-\omega;\omega,-\omega,\omega) = \gamma_{//}(-\omega;\omega,-\omega,\omega) = \frac{1}{15}\sum_{ij}^{x,y,z}\left(2\gamma_{iijj} + \gamma_{ijij}\right) \quad (4)$$

(iii) The phase-conjugate interferometry (PCI) experiment. This technique also probes $\gamma(-\omega;\omega,-\omega,\omega)$[16]. When the polarizations of the probe and of the pump are parallel, the probed second hyperpolarizability is identical to DFWM:

$$\gamma_{PCI}(-\omega;\omega,-\omega,\omega)=\gamma_{//}(-\omega;\omega,-\omega,\omega)=\frac{1}{15}\sum_{ij}^{x,y,z}\left(2\gamma_{iijj}+\gamma_{ijij}\right) \quad (5)$$

When they are orthogonally polarized, it becomes:[59]

$$\gamma_{PCI}(-\omega;\omega,-\omega,\omega)=\gamma_{\perp}(-\omega;\omega,-\omega,\omega)=\frac{1}{30}\sum_{ij}^{x,y,z}\left(3\gamma_{iijj}-\gamma_{ijij}\right) \quad (6)$$

(iv) The Kerr experiment.[60–62] In this technique, the DC field creates a refractive index difference for the parallel and perpendicular polarization. The $\gamma_{dc-Kerr}(-\omega;\omega,0,0)$ quantity is determined from analyzing the measured molar Kerr constant:[59,63,64]

$$\gamma_{dc-Kerr}(-\omega;\omega,0,0)=\frac{3}{2}\left(\gamma_{//}(-\omega;\omega,0,0)-\gamma_{\perp}(-\omega;\omega,0,0)\right)=\frac{1}{10}\sum_{ij}^{x,y,z}\left(3\gamma_{ijij}-\gamma_{iijj}\right) \quad (7)$$

(v) In third-harmonic generation (THG)[65] experiments, a ω pulsed laser beam is focused into the sample and the frequency-tripled light at 3ω is detected. It allows determining $\gamma_{\mathrm{THG}}(-3\omega;\omega,\omega,\omega)$, which reads:[65–68]

$$\gamma_{\mathrm{THG}}(-3\omega;\omega,\omega,\omega)=\gamma_{//}(-3\omega;\omega,\omega,\omega)=\frac{1}{15}\sum_{ij}^{x,y,z}3\gamma_{iijj} \quad (8)$$

Note that, like in PCI and dc-Kerr experiments, it is also possible to use orthogonally polarized incident lights with EFISHG, DFWM and THG. In all cases, away from electronic resonances, $\gamma_{//}=3\gamma_{\perp}$.[69]

(vi) The third-harmonic scattering (THS).[14,15] In this experiment, a scattered light is detected at the optical frequency 3ω from an intense laser pulsed at ω. The total third-order response reads:

$$\gamma_{THS}(-3\omega;\omega,\omega,\omega)=[\langle\gamma^2_{ZZZZ}\rangle+\langle\gamma^2_{ZXXX}\rangle]^{\frac{1}{2}} \quad (9)$$

where $\langle\gamma^2_{\mathrm{ZZZZ}}\rangle$ and $\langle\gamma^2_{\mathrm{ZXXX}}\rangle$ are rotational averages of the γ tensor components. These quantities refer to an experimental set-up where the incident light, propagating along the Y-direction, is vertically-polarized while the collected scattered light, in the X direction, is vertically-polarized [$\langle\gamma^2_{ZZZZ}\rangle$] or

View Article Online
DOI: 10.1039/D4CP00522H

horizontally-polarized [$\langle\gamma^2_{ZXXX}\rangle$]. Their ratio, known as the depolarization ratio ($\mathrm{DR}_{THS} = \langle\gamma^2_{ZZZZ}\rangle/\langle\gamma^2_{ZXXX}\rangle$), takes specific values depending on the symmetry of the molecular moiety that is responsible of the NLO responses. Assuming Kleinman's symmetry conditions, the γ tensor can be decomposed into three multipolar invariants, the isotropic (J=0), the quadrupolar (J=2) and the hexadecapolar (J=4) components so that the rotational averages and DR_{THS} become:[70]

$$\langle\gamma^2_{ZZZZ}\rangle = \frac{1}{5}\left|\gamma_{J=0}\right|^2 + \frac{4}{35}\left|\gamma_{J=2}\right|^2 + \frac{8}{315}\left|\gamma_{J=4}\right|^2 \quad (10)$$

$$\langle\gamma^2_{ZXXX}\rangle = \frac{3}{140}\left|\gamma_{J=2}\right|^2 + \frac{1}{63}\left|\gamma_{J=4}\right|^2 \quad (11)$$

$$\mathrm{DR}_{THS} = \frac{32\rho^2_{4/2} + 235\rho^2_{0/2} + 144}{20\rho^2_{4/2} + 27} \quad (12)$$

where $\rho_{0/2} = \left|\gamma_{J=0}\right|/\left|\gamma_{J=2}\right|$ and $\rho_{4/2} = \left|\gamma_{J=4}\right|/\left|\gamma_{J=2}\right|$ define the relative contributions of the spherical tensor components to the total third harmonic responses. More details on the rotational averages can be found in SI.

II.B. Computational methods

The *trans*-stilbene and *cis*-stilbene molecular structures were fully optimized at the MP2/6-311G(d) level with thresholds of 1.5×10^{-5} Hartree. Bohr $^{-1}$ and 6.0×10^{-5} Å on the forces and displacements, respectively. The harmonic vibrational frequencies were then calculated and found all real, indicating that the optimized structures are true minima on the potential energy surface (structures and energies are provided in Table S1). These optimized structures were used in all subsequent calculations.

The static γ values were evaluated with a broad range of WF methods,[71] namely HF, MP2, MP3 as well as MP4 and some intermediate levels or approximation like MP4D, MP4DQ and MP4SDQ. At the CC level, CCSD and CCSD(T) methods were employed. At the DFT level, a broad range of XCFs were used. Starting with the local density approximation (LDA) by using SVWN and improving it either with the inclusion of gradient corrections (generalized-gradient approximation, GGA) by employing BLYP, PBE and B97D XCFs or also of its kinetic energy density (meta-GGA) with M06-L. Subsequently, to provide the correct asymptotic behavior, exact Hartree-Fock exchange was included either through global hybrid (GH) or range-separated hybrid (RSH) functionals. The selected GH functionals are B3LYP (20%), PBE0 (25%), M06 (27%), M06-2X (54%), M06-HF (100%), and MN15 (44%) while the RSH functionals are ωB97, ωB97X, ωB97X-D, LC-ωPBE, LC-BLYP. The latter bring 100% of HF exchange at infinite interelectronic distances and 0% (μ =

$0.40\ \text{Bohr}^{-1}$), 15.2% ($\mu = 0.30\ \text{Bohr}^{-1}$, 22.2% ($\mu = 0.20\ \text{Bohr}^{-1}$), 0% ($\mu = 0.40\ \text{Bohr}^{-1}$), and 0% ($\mu = 0.47\ \text{Bohr}^{-1}$) of HF exchange at short ranges, respectively. The CAM-B3LYP functional which uses the Coulomb-attenuating method with 19% of HF exchange at short range and 65% at long range ($\mu = 0.33\ \text{Bohr}^{-1}$) was also considered. In addition to calculations using these standard μ values (in RSH), we carried out calculations by tuning μ in order to assess its impact as well as to determine its optimal value. Moreover, the correlation part in the DFT was also "improved" by means of second-order perturbation theory (PT2) correlation mixed with the pure DFT correlation through double hybrid (DH) XC functionals.[72,73] Here, we focus on B2-PLYP XCF that includes 27% of PT2 correlation and 53% of HF exchange, PBE0-DH (PT2 correlation: 12.5% and HF exchange: 50%), and mPW2PLYP (PT2 correlation: 25% and HF exchange: 55%). Since these combinations of PT2 correlation and HF exchange components were originally optimized based on thermodynamical data, little is known regarding their impact on the linear and nonlinear optical properties. Accordingly, the amount of PT2 correlation and HF exchange was also varied for the B2-PLYP DH functional. To determine precise γ values, the effect of the denseness of the integration grid employed in DFT calculations was assessed. Comparisons showed that employing the **superfine** or **ultrafine** integration grids (as implemented in Gaussian 16 packages[74]) provide similar values with differences smaller than <0.1% (Table S2). Then, because it is not computationally much costly (about 50% more than the ultrafine grid), all DFT calculations were performed with the **superfine** grid.

The γ tensor elements were calculated by using numerical derivative approaches,[75] known as the finite field (FF) method.[76] They were obtained by employing either the *pure numerical differentiation approach* i.e., the fourth-order derivative of field-dependent energies ($\mathcal{E}$ as defined in Eq. (13)) or the *hybrid differentiation scheme*, which consists in evaluating the second-order derivatives of α or the first-order derivatives of β as shown in Eq. (14), with α and β calculated analytically. All the details can be found in Ref. 49.

$$\gamma_{ijkl} = -\left(\frac{\partial^4 \mathcal{E}}{\partial E_i\, \partial E_j\, \partial E_k\, \partial E_l}\right)_{\vec{\mathrm{E}}\to 0} \tag{13}$$

$$\gamma_{ijkl} = \left(\frac{\partial^2 \alpha_{ij}}{\partial E_k \partial E_l}\right)_{\vec{\mathrm{E}}\to 0} = \left(\frac{\partial \beta_{ijk}}{\partial E_l}\right)_{\vec{\mathrm{E}}\to 0} \tag{14}$$

Eq. (13) was employed to calculate the static γ values with the WF methods. Thus, the field-dependent energies were calculated at different field amplitudes, with a threshold of 10^{-10} a.u. on the SCF energy. With DFT methods (with the exception of the DH XCFs), the static $[\alpha(0;0)$ and $\beta(0;0,0)]$ and dynamic $[\alpha(-\omega;\omega),\ \beta(-\omega;\omega,0),$ and $\beta(-2\omega;\omega,\omega)]$ polarizability and hyperpolarizability tensors were evaluated for different field amplitudes, at the coupled-perturbed Kohn–Sham (CPKS) and time-dependent DFT (TDDFT) levels, respectively. Then, Eq. (14) was

View Article Online
DOI: 10.1039/D4CP00522H

used to obtain the static $[\gamma(0;0,0,0)]$ and dynamic $[\gamma(-\omega;\omega,0,0),$ and $\gamma(-2\omega;\omega,\omega,0)]$ second hyperpolarizabilities. When employing DH functionals, due to the lack of analytical expressions for the linear and quadratic response functions, only the static quantities were calculated from the differentiation of the static α.

The convergence threshold on the responses of the density matrix was set to 10^{-10} a.u. Photon energies ($\hbar\omega$) range from $\hbar\omega = 0$ eV to $\hbar\omega$ = 2.72 eV ($\lambda = 456$ nm). Then, the following frequency dispersion expression, which holds for the average γ ($\gamma_{//}$ and $\gamma_{\perp}$) as well as for diagonal tensor elements was applied to estimate by fitting the A, B, … expansion coefficients:[77–79]

$$\gamma(-\omega_\sigma;\ \omega_1,\omega_2,\omega_3) = \gamma(0;0,0,0)[1 + A\omega_L^2 + B\omega_L^4 + \cdots] \quad (15)$$

$\omega_L^n = \sum_i^{\sigma,1,2,3} \omega_i^n$ (n = 2, 4, …) corresponds to the effective frequency at power "n". Though A is system-dependent, it is the same for all the third-order phenomena. Then, the A value determined from the dc-Kerr and EFISHG γ frequency dispersions were used to estimate the DFWM and THG/THS responses (the detail on the calculation of frequency-dependent THS values is provided in SI).

The solvent [1,2-dichloroethane (1,2-DCE), tetrahydrofuran (THF), chloroform, and benzene selected in agreement with experiments] effects were described by employing the solvation model density (SMD) continuum model due to Truhlar and co-workers.[80] The static dielectric constant ϵ_0 of 1,2-DCE, THF, chloroform and benzene, is equal to 10.125, 7.426, 4.711 and 2.271 while the optical one, ϵ_∞, reduces to 2.087, 1.974, 2.091 and 2.253, respectively. Note that the γ values calculated *in vacuo* employed the geometries optimized *in vacuo*, and *vice versa* for the γ values calculated in solvents. In absence of external electric field perturbation this method accounts for the self-consistent reaction field effects between the solute and the solvent molecules, described by a continuum. When calculating the responses to external (static or dynamic) electric fields, the field-induced self-consistent reaction field effects are also considered. On the other hand, cavity field factors are not taken into account.

The numerical derivative schemes employed a fully automatized Romberg scheme[81–84] in order to control and improve the accuracy and the precision on the derivatives. When the γ values are obtained as 4th-order derivatives of the energies, the stability window is small whereas it is larger for the *hybrid numerical differentiation* technique. Accordingly, in the former case, the field amplitudes were generated from the geometric progression formula $E^{k,n} = \mathrm{a}^{\frac{k}{n}} \times E_0$ with $E_0 = 6 \times 10^{-4}$ a. u., $a = 2$, $n = 2$, and $\mathrm{k} = 0, 1, 2, \ldots 8$, while $E_0 = 3 \times 10^{-4}$ a. u., $a = 2$, $n = 1$, and $\mathrm{k} = 0, 1, 2, \ldots 5$ for the latter situation. It turned out that when employing the *pure* or *hybrid numerical differentiation* approaches, the stability region of the static γ components is located in the **(k,m) = (2,2)** region (Tables S3-S5). The order of magnitude of the γ values being about 100.0×10^3 a.u. (50.0×10^3

View Article Online
DOI: 10.1039/D4CP00522H

a.u.) for the *trans* (*cis*) isomer achieving a numerical precision of 10^1 a.u. is largely enough for the current objective. One should notice that the numerical precision is better (1 a.u. or less) when adopting the *hybrid differentiation* schemes (Table S6**)** i.e., using Eq. (14). The *hybrid differentiation* approach was adopted at the DFT level, using field-dependent polarizabilities.

All the calculations were performed using the Gaussian16 program.[74] The γ values are reported in atomic units (1 a.u. of $\gamma = 6.235377 \times 10^{-65}$ $C^4m^4J^{-3} = 5.0367 \times 10^{-40}$ esu) and within the T convention.[23]

III. Results and discussion

III.A. Basis set effects

The basis set effects were assessed at the CPKS//CAM-B3LYP XCF level of approximation. All the values for EFISHG ($\gamma_{//}$) and THS (γ_{THS}, DR_{THS}) are reported in Tables S7&S8. As sketched for the Dunning basis sets in Fig. 2, the inclusion of the diffuse functions has large effect on γ while the effect of adding supplementary sets of valence functions is negligible. These conclusions hold also for Pople's basis set families. Among Pople's basis sets, the 6-311+G(d) basis set, with more than three times fewer Gaussian functions than the largest d-aug-cc-pVTZ basis set, performs well with γ underestimations of only a few percent (Fig.2 or Tables S7&S8). Negligible deviation was also observed for DR_{THS}. The γ(trans)/γ(cis) ratio decreases with increasing the basis set size. $\gamma_{//}(trans)/\gamma_{//}(cis)$ [$\gamma_{THS}(trans)/\gamma_{THS}(cis)$] goes from 3.50 [4.52] with 6-31G(d) to 2.19 [2.96] with 6-311+G(d), and to 2.17 [2.93] with d-aug-cc-pVTZ. Again, as shown in Fig. 3 (or in Table S9), 6-311+G(d) gives an excellent agreement with the largest basis set, d-aug-cc-pVTZ. From these calculations, the 6-311+G(d) basis set was selected for the rest of this study.

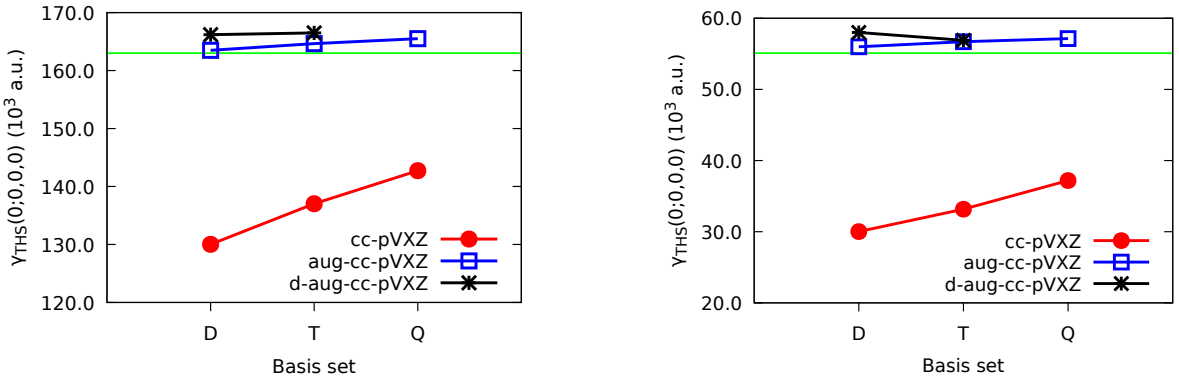

FIG. 2. Basis set effects on the static γ of *trans*- (left) and *cis*-stilbene (right) as obtained with the CAM-B3LYP XCF. The horizontal green line corresponds to 6-311+G(d) results.

View Article Online
DOI: 10.1039/D4CP00522H

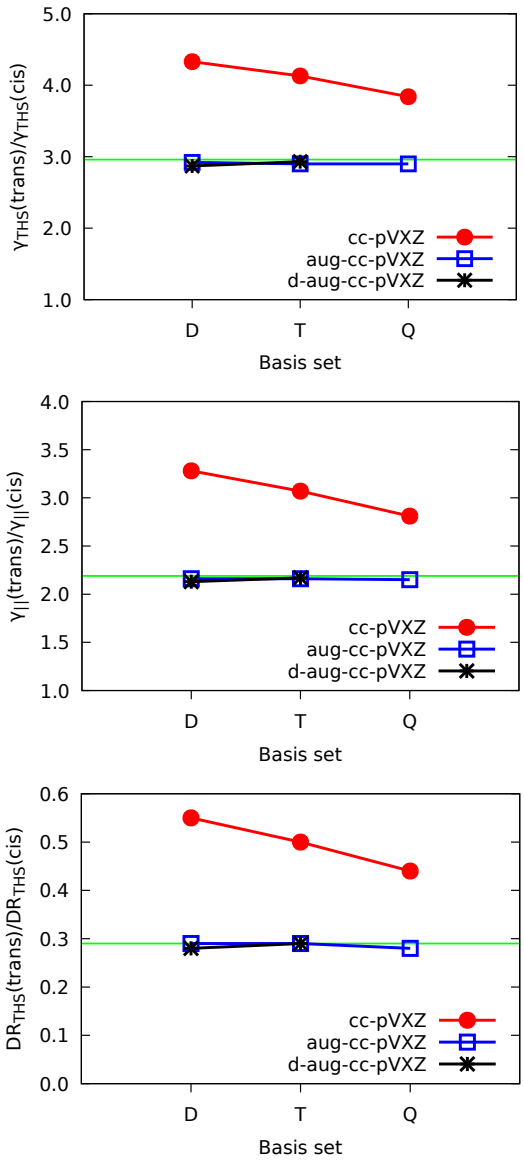

FIG. 3. Basis set effects on the $\gamma_{//}(trans)/\gamma_{//}(cis)$ (top), $\gamma_{THS}(trans)/\gamma_{THS}(cis)$ (middle), and $\mathrm{DR}_{THS}(trans)/\mathrm{DR}_{THS}(cis)$ (bottom) ratios as obtained with the CAM-B3LYP functional. The horizontal green line corresponds to 6-311+G(d) results.

III.B. Electron correlation effects

The impact of electron correlation was addressed on the static EFISHG ($\gamma_{//}$) and THS (γ_{THS}) quantities as well as on the DR_{THS} (Table 1). Depending on the method, γ is either overestimated or underestimated. With the HF method, γ is systematically underestimated (the error is the largest and amounts to ~30%), stressing again that the electron correlation effects are far from being negligible when calculating γ. The MP2 and MP4 methods overestimate the second hyperpolarizabilities but by less than 12% (6%) for the *trans* (*cis*) form. On the other hand, MP3 performs poorly with respect to MP2. Within the MP4 approximations, MP4DQ shows also some drawbacks while MP4D and MP4SDQ perform better. By including the fourth-order triple excitations into the MP4SDQ to get the complete MP4 method, the second hyperpolarizabilities increase by about 14%-16%. CCSD also

View Article Online
DOI: 10.1039/D4CP00522H

underperforms with respect to MP2 and the difference between the CCSD and CCSD(T) results reflects again the significant contribution of the triple excitations, which amounts to 10%. So, higher-order single, double and triple excitations provide positive contribution and are partially counterbalanced by quadruple excitations. This was also observed for *p*-nitroaniline.[49] Considering the DR_{THS} values, the agreement between the methods is very good for the *trans* isomer whereas for the *cis* one, HF shows strong overestimation. Moreover, MP4D and MP4 are less accurate than MP2. Looking at the switching contrasts between the *trans* and *cis* forms, the $\gamma(\text{trans})/\gamma(\text{cis})$ ratio reaches 2.0 for $\gamma_{//}$ and 2.7 for γ_{THS} at the reference CCSD(T) level (Table S10). These contrasts are well reproduced at all levels of approximation.

TABLE 1. Static second hyperpolarizabilities (10^3 a.u.) of *trans*- and *cis*-stilbene molecules as obtained with wavefunction methods using the 4^{th}-order numerical derivative approach and the 6-311+G(d) basis set. The values in the parentheses show the relative error with respect to the CCSD(T) reference.

Methods	$\gamma_{//}$	γ_{THS}	DR_{THS}
	***trans*-stilbene**		
HF	75.0 (-31)	105.0 (-32)	10.1 (2)
MP2	115.1 (7)	167.0 (8)	9.7 (-2)
MP3	97.0 (-10)	139.0 (-10)	9.9 (0)
MP4D	104.0 (-4)	149.0 (-4)	9.9 (0)
MP4DQ	96.0 (-11)	136.8 (-12)	10.1 (2)
MP4SDQ	101.6 (-6)	146.4 (-6)	9.8 (-1)
MP4	118.8 (10)	173.5 (12)	9.5 (-4)
CCSD	97.5 (-10)	138.9 (-10)	10.0 (1)
CCSD(T)	**108.0**	**155.0**	**9.9**
	***cis*-stilbene**		
HF	38.2 (-29)	40.5 (-31)	48.8 (33)
MP2	55.4 (3)	60.5 (3)	34.8 (-5)
MP3	47.8 (-11)	52.1 (-11)	35.0 (-5)
MP4D	50.8 (-6)	56.0 (-4)	33.4 (-9)
MP4DQ	48.0 (-11)	52.4 (-10)	35.7 (-3)
MP4SDQ	49.8 (-8)	54.2 (-7)	35.9 (-2)
MP4	56.2 (4)	62.0 (6)	34.0 (-8)
CCSD	49.2 (-9)	53.3 (-9)	38.5 (5)
CCSD(T)	**54.0**	**58.5**	**36.8**

III.C. Assessment of DFT exchange-correlation functionals

III.C.1. Conventional exchange-correlation functionals

The performance of DFT functionals was addressed by considering the static $\gamma_{//}$, γ_{THS} and depolarization ratio values (Table 2). The deviations on the γ values can be large, ranging from underestimations by 30% to overestimations by almost a factor of 2. The LDA and GGA XCFs

overestimate the γ values for both isomers. They show the highest overestimation errors, which amount to 58-91% (69-75%) for γ_{THS} ($\gamma_{//}$) for *trans* form while they are about 9-64% (8-54%) for *cis*. This leads to the conclusion that the consideration of the gradient of the electron density with respect to LDA do not improve the γ values. These results contrast with those on *p*NA,[49] where underestimations are smaller and of the order of 30%. Then, M06-L which includes the contribution from the kinetic energy density performs slightly better. Within hybrid functional families, GHs incorporating small amount of HF exchange also overestimate γ, but the overestimation decreases with the amount of HF exchange (Fig.4). Consequently, M06-HF shows the opposite effect and the largest underestimation as it includes the largest amount (100%) of HF exchange. Comparing M06-HF and HF method, the remaining difference is related to the correlation functional, which has a minor impact on the γ values (an increase of about 5%).

The RSH functionals also underestimate the second hyperpolarizabilities, except CAM-B3LYP for the *trans* isomer. LC-ωPBE and LC-BLYP show the highest underestimation [22-30% (24-30%) on γ_{THS} ($\gamma_{//}$)], which is consistent with their largest amount of HF exchange: at long-range, it attains 100% while their range-separating parameter amounts to 0.40 and 0.47 Bohr^{-1}, respectively. In parallel, ωB97X-D with μ =0.20 Bohr^{-1} leads to γ underestimations that remain below 10%.

For both isomers, γ are overestimated with the selected DH functionals (except PBE0-DH, which underestimates the γ values of the *cis* form). In fact, the selected three DHs differ little by the amount of HF exchange but the amount of PT2 correlation is about twice larger for mPW2-PLYP and B2-PLYP than PBE0-DH. This difference appears at the origin of the smaller overestimation of the γ values of the *trans* form and the small underestimations of those of the *cis* form, when using the PBE0-DH XCF.

Among all the selected functionals, the performance of the Minnesota XCFs depends strongly on the target system. M06-2X, ωB97X-D, and CAM-B3LYP perform better for *trans*-stilbene whereas for *cis*-stilbene, MN15, ωB97X-D, and CAM-B3LYP provide the most accurate γ values (the errors are less than 10%). From these discussions, ωB97X-D and CAM-B3LYP are recommended for the calculation of the second hyperpolarizabilities of the stilbene molecule.

For *trans*-stilbene, the DR_{THS} ranges from 8.0 to 9.6 and from 18 to 38.3 for *trans* and *cis*-stilbene, depending on the functionals. For *trans*-stilbene the largest deviation is observed for M06-L, with almost a 20% underestimation. On the other hand, most functionals perform well, with errors smaller than 10% with some GHs and RSHs. The latter XCFs are also the most reliable for predicting DR_{THS} of *cis*-stilbene but larger deviations (underestimations by up to 20-50%) are found with LDA and GGA XCFs.

TABLE 2. Static second hyperpolarizabilities (10^3 a.u.) of the *trans- and cis*-stilbene molecule, as obtained using various DFT XCFs and the 2nd order numerical derivative approach. All calculations were performed using the 6-311+G(d) basis set and the superfine grid. The values in the parentheses show the relative error with respect to the CCSD(T)/6-311+G(d) reference values (last line), obtained using the 4^{th} order numerical derivative approach.

	***trans*-stilbene**			***cis*-stilbene**		
XCFs	$\gamma_{//}$	γ_{THS}	DR_{THS}	$\gamma_{//}$	γ_{THS}	DR_{THS}
SVWN	182.4 (69)	285.2 (84)	8.4 (-15)	77.1 (43)	90.4 (55)	20.5 (-44)
BLYP	191.6 (77)	296.6 (91)	8.5 (-14)	83.0 (54)	96.1 (64)	22.1 (-40)
PBE	185.2 (71)	288.0 (85)	8.5 (-14)	79.5 (47)	92.3 (58)	21.6 (-41)
B97-D	185.0 (71)	287.0 (85)	8.5 (-14)	79.4 (47)	92.1 (57)	21.7 (-41)
M06-L	153.0 (42)	244.7 (58)	8.0 (-19)	58.5 (8)	69.7 (19)	18.8 (-49)
B3LYP	149.1 (38)	228.1 (47)	8.7 (-12)	64.8 (20)	73.5 (26)	25.2 (-32)
PBE0	136.7 (27)	209.3 (35)	8.7 (-12)	59.1 (9)	66.9 (14)	25.5 (-31)
M06	136.5 (26)	211.5 (36)	8.5 (-14)	57.2 (6)	65.5 (12)	23.7 (-36)
M06-2X	107.4 (-1)	162.7 (5)	8.8 (-11)	47.2 (-13)	52.7 (-10)	28.3 (-23)
M06-HF	82.5 (-24)	119.6 (-23)	9.6 (-3)	40.6 (-25)	44.0 (-25)	38.3 (4)
M11	87.0 (-19)	131.3 (-15)	8.9 (-10)	38.8 (-28)	43.0 (-26)	30.0 (-18)
MN15	120.1 (11)	180.1 (16)	9.0 (-9)	53.7 (-1)	59.7 (2)	29.1 (-21)
ωB97	84.8 (-21)	123.7 (-20)	9.4 (-5)	40.0 (-26)	43.4 (-26)	36.7 (0)
ωB97X	92.2 (-15)	134.1 (-13)	9.5 (-4)	44.4 (-18)	48.2 (-18)	36.7 (0)
ωB97X-D	103.6 (-4)	152.5 (-2)	9.3 (-6)	49.1 (-9)	54.0 (-8)	32.6 (-11)
LC-ωPBE	82.2 (-24)	121.5 (-22)	9.2 (-7)	37.7 (-30)	41.2 (-30)	34.6 (-6)
CAM-B3LYP	109.1 (1)	162.7 (5)	9.1 (-8)	49.9 (-8)	55.1 (-6)	31.5 (-14)
LC-BLYP	81.4 (-25)	119.3 (-23)	9.3 (-6)	38.4 (-29)	41.6 (-29)	36.9 (0)
PBE0-DH	118.4 (10)	179.2 (16)	8.8 (-11)	47.6 (-12)	51.9 (-11)	35.1 (-5)
mPW2PLYP	129.5 (20)	195.2 (26)	8.9 (-10)	57.8 (7)	64.4 (10)	29.0 (-21)
B2-PLYP	135.1 (25)	203.4 (31)	8.9 (-10)	60.2 (11)	67.1 (15)	28.9 (-21)
CCSD(T)	108.0	155.0	9.9	54.0	58.5	36.8

View Article Online
DOI: 10.1039/D4CP00522H

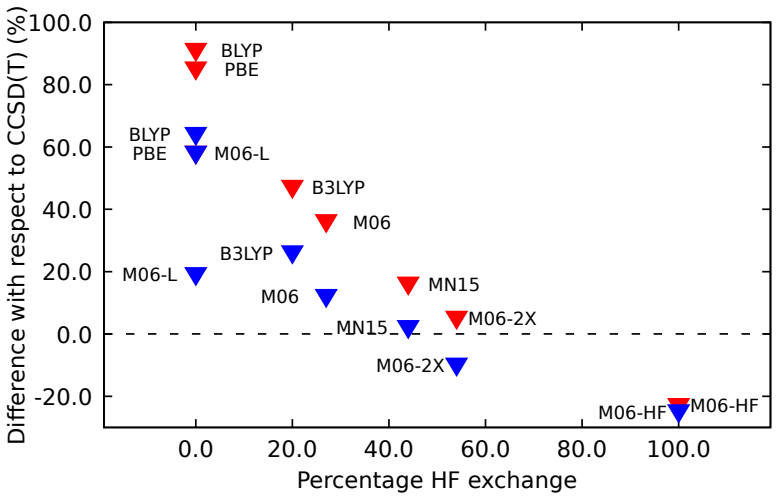

FIG. 4. Relationship between γ_{THS} for *trans*- (red) and *cis*-stilbene (blue) and the percentage of HF exchange in global hybrid XCFs. The dotted line corresponds to the reference CCSD(T) value.

All XCFs overestimate the $\gamma(trans)/\gamma(cis)$ ratio (Table S11), with typical values of 2.2 and 3.0 for $\gamma_{//}$ and γ_{THS}, respectively. The largest error corresponds to LDA, GGA, mGGA but also GH and DF XCFs. Large amount of HF exchange, using GHs or RSHs, generally improves the agreement with the reference CCSD(T) values. Among the considered functionals, M06-HF, ωB97, ωB97X, ωB97X-D, and LC-BLYP provide the best estimates of the γ(trans)/γ(cis) ratio.

Looking at the multipolar contributions, the quadrupolar one is dominant for *trans*-stilbene and it depends little on the method (Table 3 and Table S12). Then comes the isotropic component. Differences are larger for *cis*-stilbene, where the isotropic component is about twice larger than the quadrupolar one and the latter is again about twice larger than the hexadecapolar. Note that the $\rho_{0/2}$ ratio is underestimated when using LDA while it is overestimated at the HF level.

TABLE 3. Relative contribution of the isotropic, quadrupolar, and hexadecapolar components to γ_{THS} calculated at different levels of approximation with the 6-311+G(d) basis set.

Methods	***trans*-stilbene**		***cis*-stilbene**	
	$\rho_{0/2}$	$\rho_{4/2}$	$\rho_{0/2}$	$\rho_{4/2}$
SVWN	0.72	0.61	1.39	0.45
B3LYP	0.75	0.60	1.59	0.46
M06-2X	0.76	0.61	1.71	0.46
CAM-B3LYP	0.79	0.61	1.83	0.48
LC-BLYP	0.81	0.61	2.03	0.51
HF	0.87	0.62	2.46	0.61
MP2	0.83	0.57	1.93	0.46
CCSD(T)	0.84	0.57	1.97	0.43

View Article Online
DOI: 10.1039/D4CP00522H

III.C.2. Optimal tuning of the range-separating parameter

A proposition to improve the quality of a RSH XCF is to tune its range-separating parameter so that Koopmans' theorem is satisfied for the first ionization.[85,86] The details of the procedure are provided in the ESI. Figure 5a&5c sketch $\Delta_{IP}(\mu)$ [this quantity vanishes when Koopmans' theorem is fulfilled] as a function of μ with the LC-BLYP, CAM-B3LYP, and ωB97 XCFs (Table S13). In all cases, $\Delta_{IP}(\mu)$ is positive at small μ values and it decreases monotonically with μ. For LC-BLYP and ωB97, $\Delta_{IP}(\mu)$ crosses the zero line at $\mu \sim 0.23$ bohr^{-1} and then, it becomes more and more negative. For CAM-B3LYP, $\Delta_{IP}(\mu)$ decreases slowly but remains positive over the whole μ range. It should be noticed that similar trends were observed for the *p*NA molecule,[49] but the optimal μ values are different. This confirms the fact that the range-separating parameter μ is system-dependent.

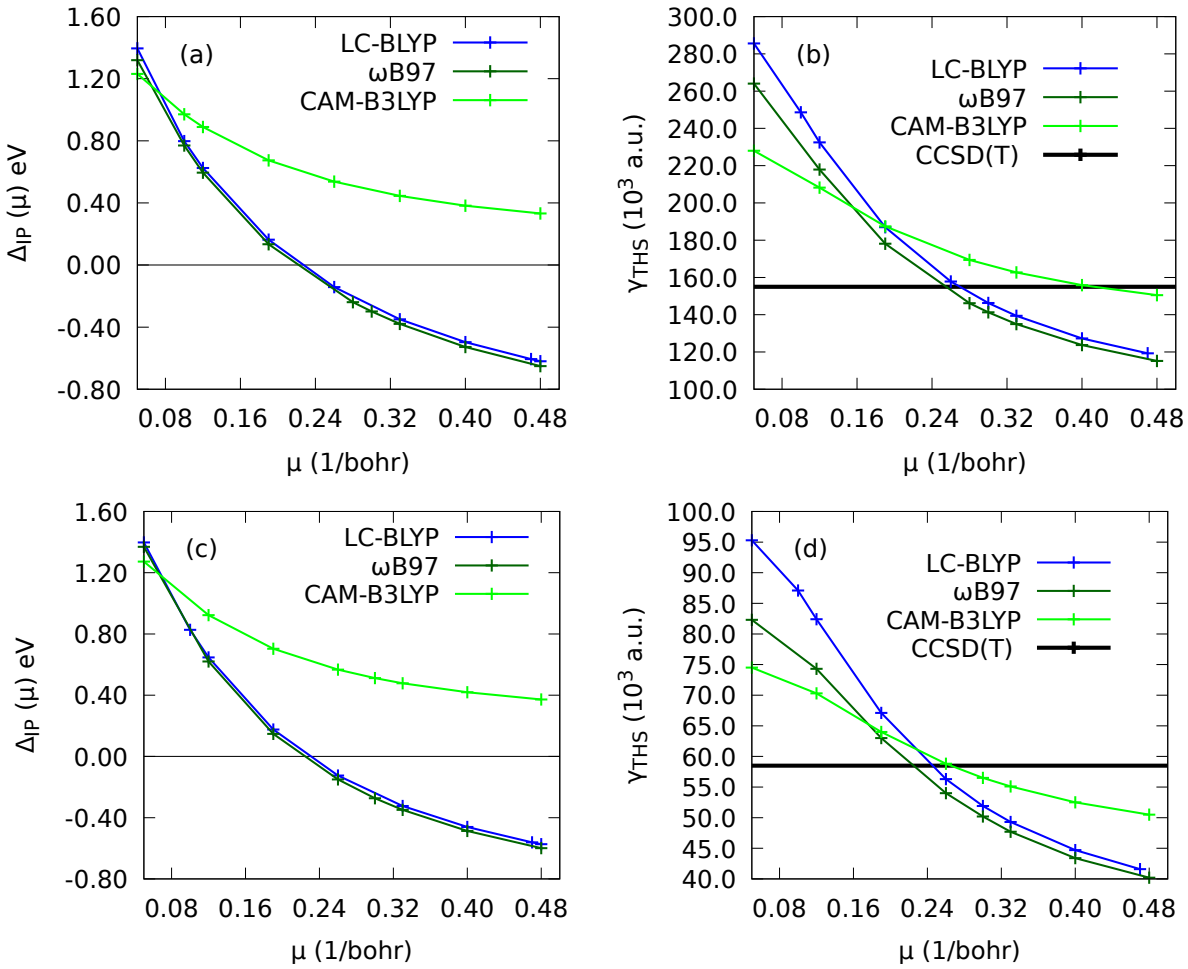

FIG. 5. Left: μ-dependence of the $\Delta_{IP}(\mu)$ function for *trans*-stilbene (a) and *cis*-stilbene (c); Right: static γ_{THS} of *trans*-stilbene (b) and *cis*-stilbene (d). The horizontal line in (a) and (c) panels correspond to $\Delta_{IP}(\mu) = 0$, *i.e.* when the Koopmans' theorem is satisfied.

γ was then calculated for the different μ values (FIG. 5b&5d or Tables S14&15). Starting from γ values that are larger than the CCSD(T) reference, for the three XCFs, γ decreases monotonically (no maximum, contrary to *p*NA[49]) until it reaches the CCSD(T) value and then, it continues to decrease.

View Article Online
DOI: 10.1039/D4CP00522H

These best μ values are equal to ~0.25 bohr^{-1} and are slightly different from the optimal ones. The use of the optimal μ values for LC-BLYP and ωB97 improves considerably the γ estimate, in comparison to the default μ values. Indeed, for *trans*-stilbene, the overestimation amounts to 6-9% on γ_{THS} and 4-6% on $\gamma_{//}$, whereas the default μ values underestimate γ by 22-25%. For the *cis* isomer, the overestimation reduces to 3-6% on γ_{THS} and 2-4% on $\gamma_{//}$ with optimal μ compared to underestimations as large as 26-29% with the default μ. For CAM-B3LYP, for which there is no μ value satisfying Koopmans' theorem, there is a μ value that reproduces the CCSD(T) result of the *trans*-stilbene (0.42 bohr^{-1}) and of the *cis*-stilbene (0.27 bohr^{-1}). Yet, as discussed above, the original CAM-B3LYP already provides accurate second hyperpolarizabilities.

The tuning procedure due to Besalú-Sala *et al.*[47] was also applied. The longitudinal polarizability values of *trans*- and *cis*-stilbene as obtained at the LC-BLYP/6-311+G* level amount to $\alpha_{xx} = 267.1$ a.u. and $\alpha_{xx} = 200.7$ a.u., respectively. This corresponds to size extensive descriptors (l_α) of 0.444 and 0.334, leading in both cases to $\mu_{\mathrm{T}\alpha} = 0.30\ \mathrm{bohr}^{-1}$ (note that the same value of $\mu_{\mathrm{T}\alpha}$ was reported for *p*NA[49]). As can be seen, the $\mu_{\mathrm{T}\alpha}$ value is larger than that obtained from Koopmans' theorem (0.23 bohr^{-1}). Thus, it underestimates the second hyperpolarizabilities of *trans*- and *cis*-stilbene. However, it performs slightly better than the original LC-BLYP XC functional.

III.C.3. Effect of the amounts of HF exchange and PT2 correlation in B2-PLYP on the second hyperpolarizability

The impact of varying the percentages of HF exchange and PT2 correlation in the B2-PLYP XCF has been analyzed on the static γ values (Figure 6, Tables S16&S17). Two tuning procedures were adopted: **i)** in the first, the % of HF exchange was kept at its default 53% value and the % of PT2 correlation was varied. For 0% of PT2 correlation, γ_{THS} amounts to 156×10^3 a.u. (53×10^3 a.u.) for the *trans* (*cis*) isomer, and then it increases linearly with the amount of PT2 correlation until it reaches a value of 337×10^3 a.u. (110×10^3 a.u.) for 100% of PT2 correlation. The best estimates of γ for the *trans* (*cis*) isomer are obtained with small amounts of PT2 correlation, 0-5% (10-15%). For comparison, the sensitivity to the dynamic correlation is smaller than for *p*NA where it was found that the original B2-PLYP XCF (27% of HF exchange; 53% of PT2 correlation) performs best.[49] **ii)** In the second, the PT2 correlation was fixed to its default value of 27% and the % of HF exchange was varied. When increasing the amount of HF exchange, γ_{THS} decreases but in a curvilinear way. Note that the curvilinear dependence of γ on the % HF exchange is due to the fact that the HF exchange term is directly involved in the SCF procedure. The γ_{THS} curves cross the CCSD(T) line with 75% (65%) of %HF for *trans* (*cis*) isomer. Therefore, the (%PT2; %HF) pairs corresponding to (27%; 75%) for the *trans* form and (27%; 65%) for the *cis*-stilbene provide the best γ estimates. From these findings, it can be concluded that, tuning the amount of HF and PT2 components in DH could

also lead to accurate γ values. Indeed, the tuned B2-PLYP improves systematically the γ values, making it to be more reliable than other XCFs, and even better than the MP2 method. Therefore, the modified B2-PLYP XCF can also be recommended for calculating the static second hyperpolarizabilities of *trans*- and *cis*-stilbene.

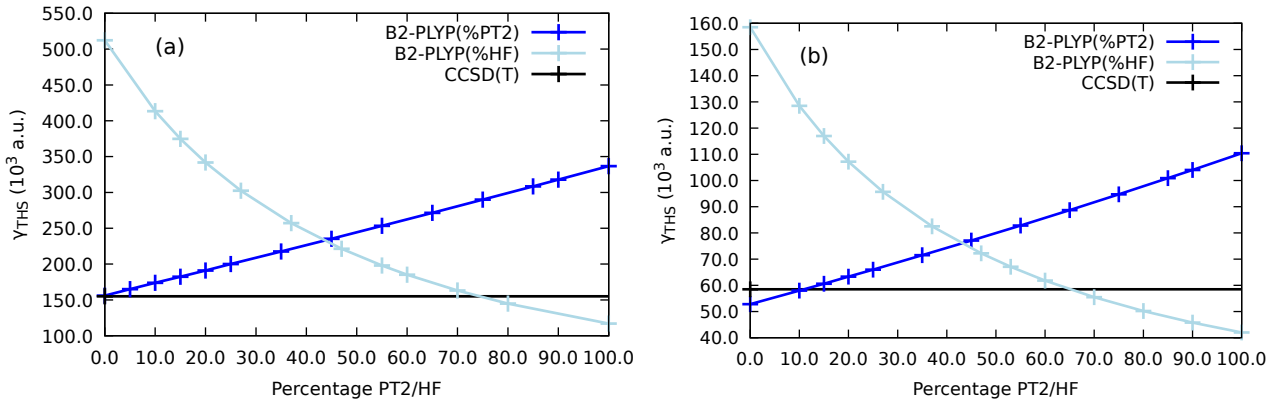

FIG. 6. Static γ_{THS} of *trans*-stilbene (a) and *cis*-stilbene (b) as a function of the percentage of PT2 correlation (keeping the %HF at its default 53% value) and as a function of the percentage of HF exchange (keeping the %PT2 at its default 27% value) in the B2-PLYP XCF.

III.C.4. Delocalization errors of XCFs versus accuracy of γ values

As a complement of these studies on the effects of the percentage of HF (GHs and RSHs) exchange and PT2 correlation, the accuracy of the γ values has been compared to the delocalization error (DE). The latter are characterized by the curvature of ΔΔε, which is the deviation from linearity of the relationship between the electronic energy and the fractional electron number (see ESI for more details). When considering the LC-BLYP XCF with μ values ranging from 0.05 to 0.48 bohr^{-1}, FIG. S3 shows that the deviation from linearity is negative (positive curvatures) for small μ values and that it increases and becomes positive (negative curvatures) for large μ values. Moreover, the smallest DEs correspond to μ~0.23 bohr^{-1}, which is in the range of μ values associated with small deviations of the γ values with respect to the reference CCSD(T) results [the best agreement with CCSD(T) being achieved with μ~0.25 bohr^{-1}]. FIG. 7 (Tables S18&19) extends the relationship between the curvature of ΔΔε and the accuracy on γ, including also LDA, GGA, meta-GGA, GH, and RSH XCFs. For the γ values of *trans*-stilbene, small curvatures (ωB97X-D and LC-BLYP with μ~0.23 bohr^{-1}) are associated with accurate responses but curvatures up to 0.7 eV (M06-2X and CAM-B3LYP) give also a good agreement with CCSD(T). The relationship between the curvature and the error on the second hyperpolarizability is almost monotonic. Then, for *cis*-stilbene, ωB97X-D and LC-BLYP with μ~0.23 bohr^{-1} also lead to small curvatures and γ errors smaller than 10% whereas MN15 performs well, though the curvature attains 1 eV. Contrary to the *trans* isomer, the relationship between the curvature and the error on the γ values is no more fully monotonic (there are values, specially for the error on $\gamma_{//}$, which do not follow an increasing trend as a function of the numerical curvature

coefficient). Considering DR_{THS}, the accuracy decreases linearly with the curvature coefficient, with a larger slope for the *cis* form.

View Article Online
DOI: 10.1039/D4CP00522H

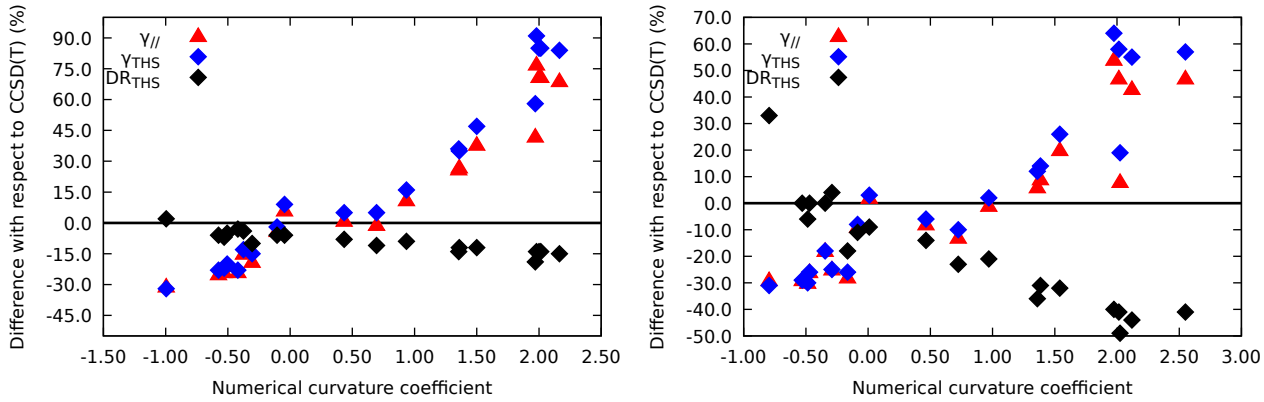

FIG. 7. Relationship between the relative errors on the γ quantities and the average numerical curvature coefficients of the $\Delta\mathcal{E}(\delta)$ *versus* δ curves, as calculated at different levels for *trans*-stilbene (left) and *cis*-stilbene (right). The horizontal line corresponds to the reference CCSD(T) value.

III.D. Solvent effects and frequency dispersion

Like for the gas phase structures, which have been used so far, the geometries of the isomers of stilbene were optimized at the MP2/6-311G(d) level by accounting for solvent (1,2-DCE, THF, chloroform, and benzene) effects with the SMD model. Solvent effects slightly destabilize the *cis* form (by almost 1 kcal/mol) with respect to the *trans* form (Table S20) and have a negligible impact on the geometries (Tables S21-S24). Note that in the following, when the second hyperpolarizabilities are calculated in a given solvent, the corresponding optimized geometry was employed.

Owing to the results and analysis of Subsection III.C., the CAM-B3LYP XCF was selected to investigate the solvent and frequency dispersion effects. First, the static γ quantities were evaluated in the different solvents, by considering either their optical (ϵ_∞) or static (ϵ_0) dielectric constants (Table S25). Calculating the static γ quantities with the solvent optical (ϵ_∞) dielectric constant is useful because it enables to monitor the evolution of the dynamic γ values as a function of the incident wavelength up to the $\lambda \rightarrow \infty$ limit. While using ϵ_∞, the static γ values increase by about 70% (*trans*) and 50% (*cis*), with small variations between the solvents because their ϵ_∞ values are almost similar (between 1.97 for THF and 2.25 for benzene). Considering ϵ_0, the enhancement reaches almost 200% for both isomers, with a strong effect of the solvent. The γ enhancements are ordered as a function of the ϵ_0 values, *i.e.* benzene < chloroform < THF < 1,2-DCE. The effects on DR_{THS} are smaller than on the γ quantities. The DR_{THS} values decrease by about 10% and are negligibly affected by the nature of the solvent. Yet, this demonstrates that the solvent has an impact on the symmetry of the NLOphore, as was previously observed for other systems.[87,88] As observed with gas phase results, the computations in the solvent media also show that γ is larger for the *trans* than for the *cis* form (Table S25), owing to the reduction of π-electron delocalization in the *cis* form.

View Article Online
DOI: 10.1039/D4CP00522H

The dynamic $\gamma_{//}(-\omega;\omega,0,0)$ and $\gamma_{//}(-2\omega;\omega,\omega,0)$ quantities of both isomers were then calculated at the CAM-B3LYP/6-311+G(d) level of approximation, *in vacuo* and in solution. Tables S26-S30 collect all the data, which have been used to plot their evolution as a function of ω as well as of ω_L^2 (FIGS. 8&9 and FIG. S4). Several observations are made: i) $\gamma_{//}(-\omega;\omega,0,0) < \gamma_{//}(-2\omega;\omega,\omega,0)$, ii) over the range of ω_L^2 values, the $\gamma_{//}(-\omega;\omega,0,0)$ and $\gamma_{//}(-2\omega;\omega,\omega,0)$ curves are almost superimposed, iii) in the small ω_L^2 region, they evolve linearly with ω_L^2, iv) the frequency dispersion of the γ quantities is stronger in solution than *in vacuo*, and v) close to halve of the excitation energies, $\gamma_{//}(-2\omega;\omega,\omega,0)$ is impacted by resonance effects and can change sign. Indeed, the first excitation energy of *trans*-stilbene [*cis*-stilbene] amounts to (3.95-4.32 eV) [4.32 (5.55)-4.49 (5.74) eV], as a function of the surrounding (Tables S33&34).

The frequency dispersions were characterized by fitting the polynomial in Eq. (15) to the data points (Table 4), where the coefficient (A) of the leading term, linear in ω_L^2, gives a first information on the relative evolution with the frequency for the different media. For both isomers, the A coefficients in solution are systematically larger than *in vacuo*, which is consistent with the enhancement of γ quantities and of their frequency dispersion. However, they remain almost similar for all solvents, which is not surprising owing to their very close optical dieletric constants. These relative values are difficult to rationalize, either in terms the first excitation energies (smaller excitation energies would be associated with larger A coefficients) or as a function of ϵ_∞ (larger A coefficients would be related to larger dielectric constants). It should also be noticed that the A value is about 50% larger for *trans*-stilbene than *cis*-stilbene, which is consistent with the previous analysis.

View Article Online
DOI: 10.1039/D4CP00522H

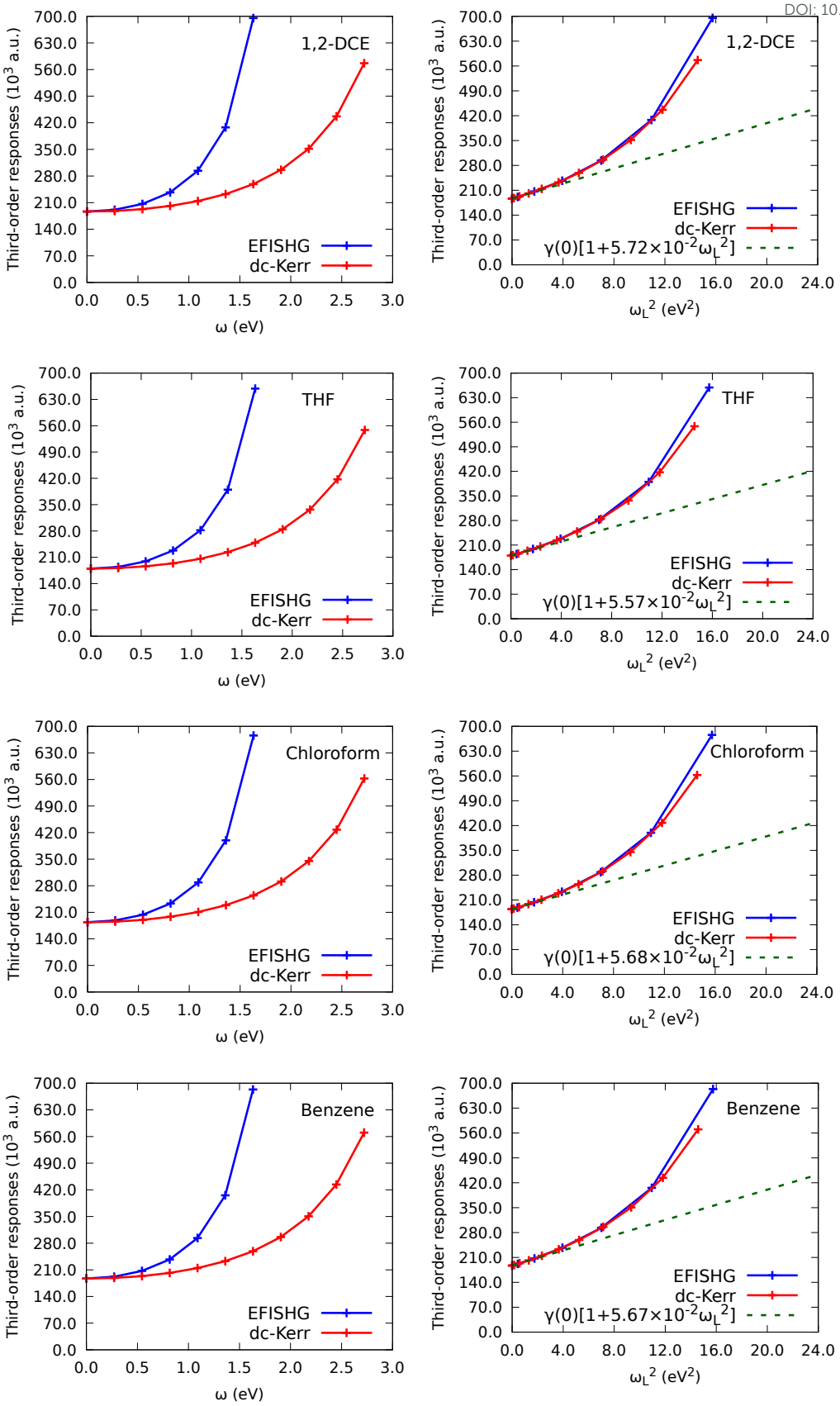

FIG 8. TDDFT/CAM-B3LYP/6-311+G(d) dc-Kerr and EFISHG second hyperpolarizabilities ($\gamma_{//}$) as a function of the frequency (left) and ω_L^2 (right) for *trans*-stilbene in 1,2-DCE, THF, chloroform and in benzene solvent media.

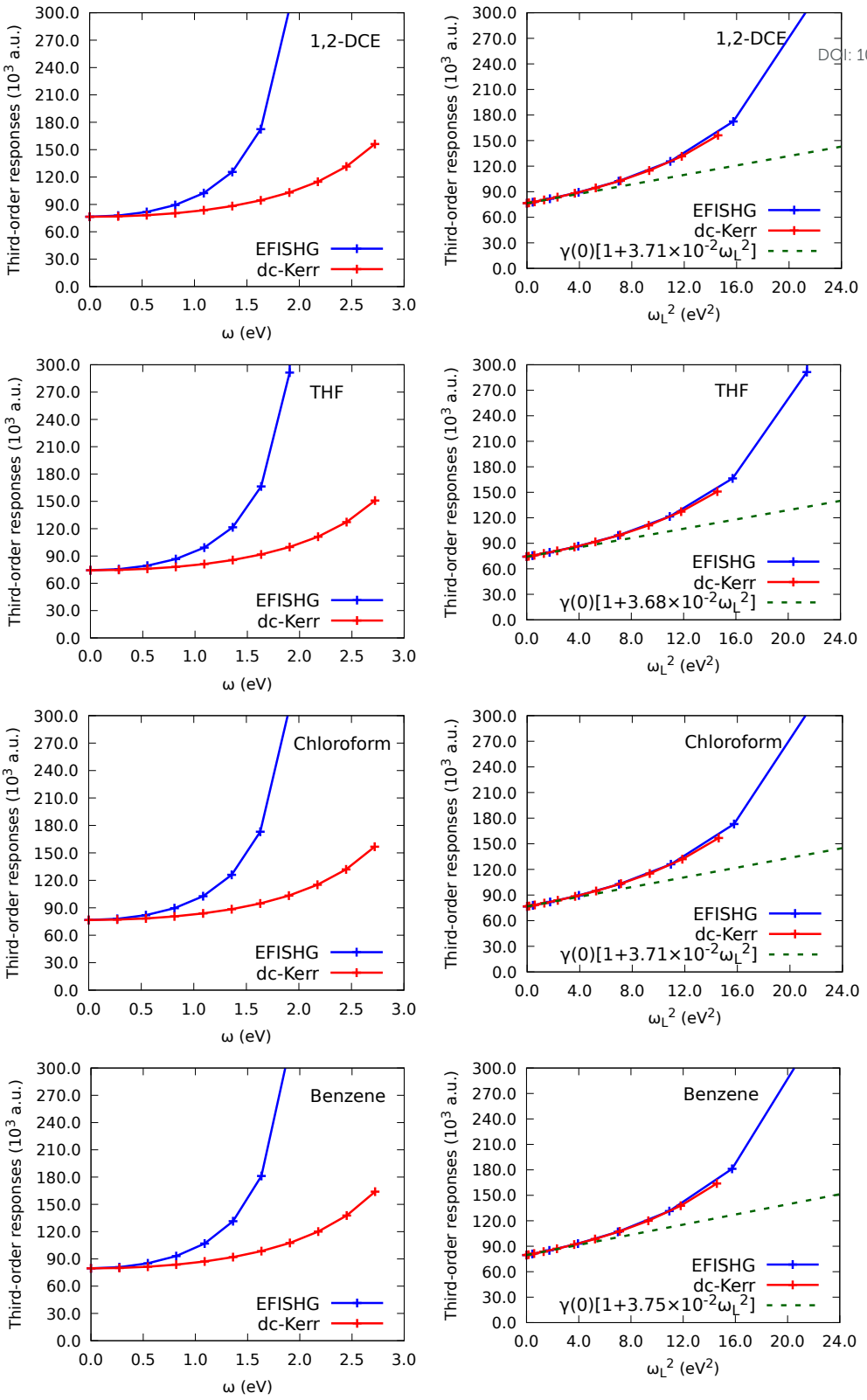

FIG 9. TDDFT/CAM-B3LYP/6-311+G(d) dc-Kerr and EFISHG second hyperpolarizabilities ($\gamma_{//}$) as a function of the frequency (left) and ω_L^2 (right) for *cis*-stilbene in 1,2-DCE, THF, chloroform and in benzene solvent media.

Since, as demonstrated by Bishop and co-workers,[77–79] the A value does not depend on the third-order NLO process, the $\gamma_{DFWM}(-\omega;\ \omega,-\omega,\omega)$ and $\gamma_{THG}(-3\omega;\ \omega,\omega,\omega)$ values could be calculated by using these linear regression relationships, provided that one remains in the linear

View Article Online
DOI: 10.1039/D4CP00522H

regime of γ as a function of ω_L^2. This is done in the next Subsection when making comparisons with experiment.

TABLE 4: Frequency dispersion expressions for $\gamma_{//}$ (10^3 a.u.) at small frequencies (before resonance) of *trans*- and *cis*-stilbene as obtained from Eq. 15 in the gas phase and in different solvents using the SMD//CAM-B3LYP/6-311+G(d) level of approximation.

	***trans*-stilbene**
in vacuo	$109.2 \times [1 + (4.88 \pm 0.01) \times 10^{-2} \times \omega_L^2(eV^2) + \cdots]$
benzene	$187.2 \times [1 + (5.67 \pm 0.03) \times 10^{-2} \times \omega_L^2(\mathrm{eV}^2) + \cdots]$
chloroform	$184.0 \times [1 + (5.68 \pm 0.04) \times 10^{-2} \times \omega_L^2(\mathrm{eV}^2) + \cdots]$
THF	$180.0 \times [1 + (5.67 \pm 0.03) \times 10^{-2} \times \omega_L^2(\mathrm{eV}^2) + \cdots]$
1,2-DCE	$186.5 \times [1 + (5.72 \pm 0.05) \times 10^{-2} \times \omega_L^2(\mathrm{eV}^2) + \cdots]$
	***cis*-stilbene**
in vacuo	$50.0 \times [1 + (3.29 \pm 0.02) \times 10^{-2} \times \omega_L^2(eV^2) + \cdots]$
benzene	$76.6 \times [1 + (3.75 \pm 0.01) \times 10^{-2} \times \omega_L^2(\mathrm{eV}^2) + \cdots]$
chloroform	$76.7 \times [1 + (3.71 \pm 0.01) \times 10^{-2} \times \omega_L^2(\mathrm{eV}^2) + \cdots]$
THF	$74.3 \times [1 + (3.68 \pm 0.01) \times 10^{-2} \times \omega_L^2(\mathrm{eV}^2) + \cdots]$
1,2-DCE	$76.5 \times [1 + (3.71 \pm 0.01) \times 10^{-2} \times \omega_L^2(\mathrm{eV}^2) + \cdots]$

III.E. Comparisons with experiment

Table 5 collects experimental second hyperpolarizabilities of *trans*-stilbene, their associated uncertainties, some aspects of their measurements, in comparison to values calculated at the SMD//CAM-B3LYP/6-311+G(d) level. As specified in the experimental papers, all the measurements have been carried out on the *trans* isomer in liquid phase. This is consistent with the relative Gibbs free energies between the two forms given in Table S20: the *cis/trans* Maxwell-Boltzmann populations at 298.15 K range from 4/96 to 2/98 as a function of the solvent. Considering Ref. 12 which reported γ values for both *trans* and *cis* stilbene, it was observed that γ of *trans* stilbene is about twice larger than that of *cis* stilbene, which agrees with the calculations (Table S25).

These experimental values have been determined by employing the external reference technique *i.e.*, the second hyperpolarizability of a reference material is used as a standard to determine the γ value of the *trans*-stilbene molecule. The reference material, as well as information on the experimental set-up are provided in Table 5. Reference γ values correspond to those of Ref. 14 (except the one from Ref. 13 that has been added). When necessary, the experimental values have been converted to the T-convention [$\gamma_T = 6\,\gamma_B$],[23] and rescaled by using the most recent calibration based on the $\chi^{(2)}$ and $\chi^{(3)}$ values of α-quartz[89] (see details in Ref. 14).

Two $\gamma(-\omega;\omega,-\omega,\omega)$ values, determined using the PCI[11] and DFWM[9] experimental techniques, are reported. However, the DFWM quantity is $\gamma_{//}(-\omega;\omega,-\omega,\omega)$ while the PCI one corresponds to $\gamma_{\perp}(-\omega;\omega,-\omega,\omega)$. Thus, besides the fact that the solvents and frequencies are different, these PCI and DFWM values cannot be compared directly. Accordingly, the theoretical PCI value was estimated from Eq. (15) applied to $\gamma_{\perp}$[77] [the dynamic $\gamma_{\perp}(-\omega;\omega,0,0)$ and $\gamma_{\perp}(-2\omega;\omega,\omega,0)$ quantities for *trans*-stilbene are gathered in Table S31 while FIG. S5 sketches their evolution as a function of frequency and of ω_L^2]. For both $\gamma(-\omega;\omega,-\omega,\omega)$ quantities, the experimental values are larger than the theoretical ones, with calc./exp. ratios of 0.5 and 0.7, respectively. Provided the different approximations are reliable, this large deviation points out to the fact that the measured quantities might not only be determined by electronic contributions. As a matter of fact, additional calculations were performed to evaluate the dominant vibrational contribution to $\gamma(-\omega;\omega,-\omega,\omega)$. In the infinite optical frequency limit,[90–93] it reads $\frac{2}{3}[\alpha^2]^0_{\omega=0}$ (details of the calculations are provided in SI). Employing the same level of approximation as for the electronic response, the so-called Raman term, $[\alpha^2]^0_{\omega=0}$, amounts to 244.2×10^3 a.u.. Adding this contribution to the electronic response substantially improves the agreement between the experimental and theoretical values. Indeed, the total DFWM $\gamma_{//}(-\omega;\omega,-\omega,\omega)$ value is equal to 515.8×10^3 a.u. (deviation of 4% with respect to experiment) while the PCI $\gamma_{\perp}(-\omega;\omega,-\omega,\omega)$ attains 196.2×10^3 a.u. (deviation of 28%). In addition, since *trans*-stilbene is a highly anisotropic molecule, the remaining difference of 28% on the PCI quantity could be related to orientational contributions that could appear in PCI measurement, especially when using ns-laser.[9,94]

In the case of EFISHG, three $\gamma_{//}(-2\omega;\omega,\omega,0)$ values were reported for the same solvent and at the same wavelength (1064 nm). Two of these, 65.5×10^3 a.u.[11] and 78.2×10^3 a.u.[13] are consistent with each other, but they differ by more than a factor of 2 from that of Ref. 12. This difference could be related to the presence of the electric field induced optical mixing nonlinearity effects producing a $2\omega+\omega=3\omega$ signal in the total response (Ref. 12) compared to the measurement performed in Ref. 13 where the third harmonic generation was eliminated by using appropriate filters. Comparison between, experiment and theory shows that the experimental values are twice or four times smaller than the calculated ones. Resonance effects cannot explain these differences because the SHG wavelength (532 nm) is far below (in energy) the first transition that peaks around 310 nm (Table S33). On the other hand, when considering the experimental value measured in chloroform at 1910 nm, the agreement with our calculations is much better, with a correction factor of only 1.4, which is within the experimental confidence interval (two standard deviations).

View Article Online
DOI: 10.1039/D4CP00522H

A THG value was measured in chloroform at a wavelength of 1910 nm, again well below resonance. Calculations predict a value that is twice larger. Moreover, comparison of the measured $\gamma_{//}(-2\omega;\omega,\omega,0)$ and $\gamma_{//}(-3\omega;\omega,\omega,\omega)$ values at the same wavelength and in the same solvent demonstrates an inconsistency between these experimental values because one expects that THG provides a larger value than EFISHG, owing to a stronger frequency dispersion. From CAM-B3LYP calculations, this difference should be of the order of 10-15%; thus if $\gamma_{//}(-2\omega;\omega,\omega,0)$=155× 10^3 one expects $\gamma_{//}(-3\omega;\omega,\omega,\omega)$ ~ 175× 10^3 a.u.. Note that the difference cannot be associated with a vibrational contribution. Indeed, the so-called IR-hyperRaman term, $[\mu\beta]^0_{\omega=0}$, amounts to 14.6 × 10^3 a.u. and the contribution to $\gamma_{//}(-2\omega;\omega,\omega,0) = \frac{1}{4}[\mu\beta]^0_{\omega=0}$= 3.7 × 10^3 (details of the calculations are provided in SI).

Finally, the calculated THS value is also much larger than the experimental one (factor of 5.6). No pre-resonance effects could be invoked to explain a difference because the incident wavelength of 1260 nm leads to third harmonic photons at 420 nm, too far from the maximum absorption wavelength of *trans*-stilbene. Since both results are associated with third harmonic generation, the $\gamma_{THS}(-3\omega;\omega,\omega,\omega)$ and $\gamma_{//}(-3\omega;\omega,\omega,\omega)$ quantities have been compared. Experimentally, the $\gamma_{THS}(-3\omega;\omega,\omega,\omega)[1260\text{ nm}]/\gamma_{//}(-3\omega;\omega,\omega,\omega)[1910\text{ nm}]$ ratio equals 0.74. On the other hand, the corresponding ratio evaluated from the IEFPCM(chloroform)/CAM-B3LYP calculations amounts to 2.09. The latter value was obtained by starting from the static $\gamma_{THS}/\gamma_{//}$ ratio of 1.55 (Table S25) and adding frequency dispersions. Indeed, the frequency factor of $\gamma_{THS}(-3\omega;\omega,\omega,\omega)[1260\text{ nm}]$ amounts to 1.74 but only to 1.29 for $\gamma_{//}(-3\omega;\omega,\omega,\omega)[1910\text{ nm}]$, which gives a value of $1.55 \times (1.74/1.29) = 2.09$ for the $\gamma_{THS}(-3\omega;\omega,\omega,\omega)[1260\text{ nm}]/\gamma_{//}(-3\omega;\omega,\omega,\omega)[1910\text{ nm}]$ ratio. This suggests that the experimental $\gamma_{THS}/\gamma_{//}$ ratio should have been much larger than 0.74.

TABLE 5. Comparison between experimental and calculated frequency-dependent second hyperpolarizabilities of *trans*-stilbene (10^3a.u., within the T convention). The values in parentheses in the last column show the deviation factor of the calculations from experiment.

Solvent	λ (nm)	NLO phenomenon	Property	Reference material	Laser pulse duration	Experiment	Calculations
1,2-DCE	532	PCI	$\gamma_{\perp}(-\omega;\omega,-\omega,\omega)$	CS_2	ns	274.0± 48.0[11]	141.9 (0.5) [196.2 (0.72)][a]
THF	602	DFWM	$\gamma_{//}(-\omega;\omega,-\omega,\omega)$	CS_2	sub-ps	495.6±58.4[9]	353.0 (0.7) [515.8 (1.04)][a]
Benzene	1064	EFISHG	$\gamma_{//}(-2\omega;\omega,\omega,0)$	α-quartz	ns	65.5±31.0[11]	274.4 (4.2)
Benzene	1064	EFISHG	$\gamma_{//}(-2\omega;\omega,\omega,0)$	α-quartz	ns	141.8±25.0[12]	274.4 (1.9)
Benzene	1064	EFISHG	$\gamma_{//}(-2\omega;\omega,\omega,0)$	α-quartz	pps	78.2±5.9[13]	274.4 (3.5)
Chloroform	1910	EFISHG	$\gamma_{//}(-2\omega;\omega,\omega,0)$	α-quartz	ns	154.9±35.7[10]	210.4 (1.4)
Chloroform	1910	THG	$\gamma_{//}(-3\omega;\omega,\omega,\omega)$	BK7	ns	119.1±23.8[10]	237.0 (2.0)
Chloroform	1260	THS	$\gamma_{THS}(-3\omega;\omega,\omega,\omega)$	CCl_4	fs	88.2±13.1[14]	492.5 (5.6)[b]

[a] values obtained after including the dominant vibrational contribution are given in square brackets.

[b] value obtained from Eq. (S19) derived using the data of Table S32.

IV. Conclusions and outlook

The second hyperpolarizability of the stilbene photochromic switch has been calculated by using a panoply of quantum chemistry methods. First, reference values have been calculated at the CCSD(T) level, demonstrating that *trans*-stilbene presents a $\gamma_{//}$ value that is twice larger than its *cis* isomer (its γ_{THS} value is 2.7 times larger). Owing to this significant contrast of second hyperpolarizability, stilbene could be exploited as a third-order molecular switch for potential optoelectronic applications such as molecular-scale memory devices with nondestructive reading capacity.[95] Indeed, the measurement of the γ response can be performed with an incident wavelength that does modify the state (*cis* or *trans*) of the molecule, i.e. that does not erase the information. Moreover, these reference CCSD(T) calculations point out that the dominant component to γ_{THS} is quadrupolar for *trans*-stilbene but isotropic for the *cis* form. Calculations using several wavefunction methods also show that the MP2 method is a computational cost-effective alternative to CCSD(T) for calculating the static responses. Then, searching for a reliable exchange-correlation functional, it was found that CAM-B3LYP and ωB97X-D provide accurate $\gamma_{//}$ and γ_{THS} values as well as depolarization ratios for both isomers. Additional analysis made the link between the accuracy of the exchange-correlation functionals, the fulfillment of Koopmans' theorem (including by tuning the range-separating parameter), and the delocalization error, demonstrating that satisfying Koopmans' theorem is not the condition for the best accuracy but that functionals with small delocalization errors are generally efficient. It was further shown that tuning the percentages of HF exchange and of second-order perturbation theory correlation can maximize the reliability of the B2-PLYP double hybrid functional. Taking advantage of this benchmarking, the CAM-B3LYP exchange-correlation functional has then been enacted to calculate the dynamic second hyperpolarizabilities *in vacuo* as well as in different solvents using the implicit solvation model density scheme. Large γ enhancements by about 70% (*trans*-stilbene) and 50% (*cis*-stilbene) have been evidenced, even for apolar solvents. In addition to the $\gamma(-\omega;\omega,0,0)$ and $\gamma(-2\omega;\omega,\omega,0)$ quantities that have been explicitly calculated, using frequency dispersion relationships, the γ quantities associated with other phenomena, $\gamma(-\omega;\ \omega,-\omega,\omega)$ and $\gamma(-3\omega;\ \omega,\omega,\omega)$, have also been estimated, allowing comparisons with experimental data from the literature. To a certain extent, there is no systematic agreement between the calculations and the measured values. On the one hand, the agreement is satisfactory for the $\gamma(-\omega;\ \omega,-\omega,\omega)$ quantities, provided the dominant vibrational contribution is taken into account. Therefore, this vibrational contribution accounts partly for the larger $\gamma(-\omega;\ \omega,-\omega,\omega)$ responses in comparison to the $\gamma(-2\omega;\omega,\omega,0)$ and $\gamma(-3\omega;\ \omega,\omega,\omega)$ ones. On the other hand, the agreement is poor for the $\gamma(-2\omega;\omega,\omega,0)$ and $\gamma(-3\omega;\ \omega,\omega,\omega)$ quantities. In these cases, comparing the experimental data among themselves highlighted inconsistencies, in particular for $\gamma(-2\omega;\omega,\omega,0)$ because the same wavelength and reference were used while for $\gamma(-3\omega;\ \omega,\omega,\omega)$ both are different. One possible direction of improvement of the quantum chemistry predictions consists in including

View Article Online
DOI: 10.1039/D4CP00522H

dynamical structural effects as well as explicit solvation effets in the calculations, like in recent works on the second harmonic scattering responses,[96] or including local/cavity field factor corrections but all inconsistencies with and between the experimental values will not disappear.

Conflicts of interest

The authors declare no competing financial interest.

Data availability

The data that support the findings of this study are available within the article and its ESI.

Acknowledgements

The calculations were performed on the computers of the « Consortium des équipements de Calcul Intensif (CÉCI) » (http://www.ceci-hpc.be), including those of the « UNamur Technological Platform of High-Performance Computing (PTCI) » (http://www.ptci.unamur.be) and those of the Tier-1 supercomputer of the Fédération Wallonie-Bruxelles, for which we gratefully acknowledge the financial support from the FNRS-FRFC, the Walloon Region, and the University of Namur (Conventions No. 2.5020.11, U.G006.15, U.G018.19, U.G011.22, RW1610468, RW/GEQ2016, 1117545, and RW2110213).

References

1 D. R. Kanis, M. A. Ratner and T. J. Marks, Design and Construction of Molecular Assemblies with Large Second-Order Optical Nonlinearities. Quantum Chemical Aspects, *Chem. Rev.*, 1994, **94**, 195–242.

2 J. M. Hales, J. Matichak, S. Barlow, S. Ohira, K. Yesudas, J.-L. Brédas, J. W. Perry and S. R. Marder, Design of Polymethine Dyes with Large Third-Order Optical Nonlinearities and Loss Figures of Merit, *Science (80-.).*, 2010, **327**, 1485–1488.

3 S. Mukhopadhyay, C. Risko, S. R. Marder and J.-L. Brédas, Polymethine dyes for all-optical switching applications: a quantum-chemical characterization of counter-ion and aggregation effects on the third-order nonlinear optical response, *Chem. Sci.*, 2012, **3**, 3103.

4 S. Barlow, J. L. Brédas, Y. A. Getmanenko, R. L. Gieseking, J. M. Hales, H. Kim, S. R. Marder, J. W. Perry, C. Risko and Y. Zhang, Polymethine materials with solid-state third-order optical susceptibilities suitable for all-optical signal-processing applications, *Mater. Horizons*, 2014, **1**, 577–581.

5 M. Irie, Photochromism: Memories and Switches Introduction, *Chem. Rev.*, 2000, **100**, 1683–1684.

6 D. H. Waldeck, Photoisomerization dynamics of stilbenes in polar solvents, *J. Mol. Liq.*, 1993, **57**, 127–148.

7 N. Tamai and H. Miyasaka, Ultrafast Dynamics of Photochromic Systems, *Chem. Rev.*,

2000, **100**, 1875–1890.
8 H. Meier, The Photochemistry of Stilbenoid Compounds and Their Role in Materials Technology, *Angew. Chemie Int. Ed.*, 1992, **31**, 1399–1420.
9 S. Ghosal, M. Samoc, P. N. Prasad and J. J. Tufariello, Optical nonlinearities of organometallic structures: Aryl and vinyl derivatives of ferrocene, *J. Phys. Chem.*, 1990, **94**, 2847–2851.
10 L. T. Cheng, W. Tam, S. H. Stevenson, G. R. Meredith, G. Rikken and S. R. Marder, Experimental investigations of organic molecular nonlinear optical polarizabilities. 1. Methods and results on benzene and stilbene derivatives, *J. Phys. Chem.*, 1991, **95**, 10631–10643.
11 A. P. Persoons, B. M. Van Wonterghem and P. C. Tackx, in *Nonlinear Optics II*, eds. R. A. Fisher and J. F. Reintjes, SPIE, 1991, vol. 1409, p. 220.
12 J. L. Oudar, Optical nonlinearities of conjugated molecules. Stilbene derivatives and highly polar aromatic compounds, *J. Chem. Phys.*, 1977, **67**, 446–457.
13 B. F. Levine and C. G. Bethea, Ultraviolet dispersion of the donor–acceptor charge transfer contribution to the second order hyperpolarizability, *J. Chem. Phys.*, 1978, **69**, 5240–5245.
14 N. Van Steerteghem, K. Clays, T. Verbiest and S. Van Cleuvenbergen, Third-Harmonic Scattering for Fast and Sensitive Screening of the Second Hyperpolarizability in Solution, *Anal. Chem.*, 2017, **89**, 2964–2971.
15 V. Rodriguez, Polarization-Resolved Third-Harmonic Scattering in Liquids, *J. Phys. Chem. C*, 2017, **121**, 8510–8514.
16 P. Tackx, M. Kauranen and A. Persoons, Determination of resonant and nonresonant third-order nonlinearities of organic molecules by phase-conjugate interferometry, *Opt. Lett.*, 1994, **19**, 1113.
17 P. Tackx, M. Kauranen and A. Persoons, Distinction of two-photon absorption from other nonlinear loss mechanisms by phase-conjugate interferometry, *Appl. Phys. Lett.*, 1994, **65**, 280–282.
18 K. D. Singer and A. F. Garito, Measurements of molecular second order optical susceptibilities using dc induced second harmonic generation, *J. Chem. Phys.*, 1981, **75**, 3572–3580.
19 I. Ledoux and J. Zyss, Influence of the molecular environment in solution measurements of the second-order optical susceptibility for urea and derivatives, *Chem. Phys.*, 1982, **73**, 203–213.
20 T. Verbiest, K. Clays and V. Rodriguez, *Second-order nonlinear optical characterization techniques*, CRC Press, Boca Raton, FL, 2009.
21 H. J. Lehmeier, W. Leupacher and A. Penzkofer, Nonresonant third order hyperpolarizability of rare gases and N2 determined by third harmonic generation, *Opt. Commun.*, 1985, **56**, 67–72.
22 L. Brzozowski and E. H. Sargent, Azobenzenes for photonic network applications: Third-order nonlinear optical properties, *J. Mater. Sci. Mater. Electron.*, 2001, **12**, 483–489.
23 H. Reis, Problems in the comparison of theoretical and experimental hyperpolarizabilities revisited, *J. Chem. Phys.*, 2006, **125**, 014506.
24 J. F. Nicoud and R. J. Twieg, in *Nonlinear optical properties of organic molecules and crystals*, 2012, vol. 1, pp. 227–296.
25 E. Perrin, P. N. Prasad, P. Mougenot and M. Dupuis, Ab initio calculations of polarizability and second hyperpolarizability in benzene including electron correlation treated by Møller–Plesset theory, *J. Chem. Phys.*, 1989, **91**, 4728–4732.
26 H. Sekino and R. J. Bartlett, Molecular hyperpolarizabilities, *J. Chem. Phys.*, 1993, **98**, 3022–3037.
27 S. Nénon, B. Champagne and M. I. Spassova, Assessing long-range corrected functionals with physically-adjusted range-separated parameters for calculating the polarizability and the

second hyperpolarizability of polydiacetylene and polybutatriene chains, *Phys. Chem. Chem. Phys.*, 2014, **16**, 7083–7088.
View Article Online
DOI: 10.1039/D4CP00522H
28 A. Mondal, K. Hatua, R. S. Roy and P. K. Nandi, Successive lithiation of acetylene, ethylene and benzene: a comprehensive computational study of large static second hyperpolarizability, *Phys. Chem. Chem. Phys.*, 2017, **19**, 4768–4777.
29 P. Beaujean and B. Champagne, Coupled cluster investigation of the vibrational and electronic second and third harmonic scattering hyperpolarizabilities of the water molecule, *J. Chem. Phys.*, 2019, **151**, 064303.
30 R. L. Beil and R. J. Hinde, Ab initio electrical properties of CO2: polarizabilities, hyperpolarizabilities, and multipole moments, *Theor. Chem. Acc.*, 2021, **140**, 120.
31 C. Naim, P. Besalú-Sala, R. Zaleśny, J. M. Luis, F. Castet and E. Matito, Are Accelerated and Enhanced Wave Function Methods Accurate to Compute Static Linear and Nonlinear Optical Properties?, *J. Chem. Theory Comput.*, 2023, **19**, 1753–1764.
32 T. T. Toto, J. L. Toto, C. P. de Melo, M. Hasan and B. Kirtman, Ab initio finite oligomer method for nonlinear optical properties of conjugated polymers. Effect of electron correlation on the static longitudinal hyperpolarizability of polyacetylene, *Chem. Phys. Lett.*, 1995, **244**, 59–64.
33 T. Kobayashi, K. Sasagane, F. Aiga and K. Yamaguchi, Calculation of frequency-dependent second hyperpolarizabilities for electric field induced second harmonic generation in the second-order Møller-Plesset perturbation theory, *J. Chem. Phys.*, 1999, **111**, 842–848.
34 B. Champagne, E. Botek, M. Nakano, T. Nitta and K. Yamaguchi, Basis set and electron correlation effects on the polarizability and second hyperpolarizability of model open-shell π-conjugated systems, *J. Chem. Phys.*, 2005, **122**, 114315.
35 G. Maroulis, On the bond-length dependence of the static electric polarizability and hyperpolarizability of F2, *Chem. Phys. Lett.*, 2007, **442**, 265–269.
36 P. Norman, A perspective on nonresonant and resonant electronic response theory for time-dependent molecular properties, *Phys. Chem. Chem. Phys.*, 2011, **13**, 20519–20535.
37 P. A. Limacher, Q. Li and H. P. Lüthi, On the effect of electron correlation on the static second hyperpolarizability of π conjugated oligomer chains, *J. Chem. Phys.*, 2011, **135**, 014111.
38 A. Avramopoulos, H. Reis, J. M. Luis and M. G. Papadopoulos, On the vibrational linear and nonlinear optical properties of compounds involving noble gas atoms: HXeOXeH, HXeOXeF, and FXeOXeF, *J. Comput. Chem.*, 2013, **34**, 1446–1455.
39 J. P. Coe and M. J. Paterson, Approaching exact hyperpolarizabilities via sum-over-states Monte Carlo configuration interaction, *J. Chem. Phys.*, 2014, **141**, 124118.
40 B. Champagne, E. A. Perpète, S. J. A. van Gisbergen, E.-J. Baerends, J. G. Snijders, C. Soubra-Ghaoui, K. A. Robins and B. Kirtman, Erratum: "Assessment of conventional density functional schemes for computing the polarizabilities and hyperpolarizabilities of conjugated oligomers: An ab initio investigation of polyacetylene chains" [J. Chem. Phys. 109 , 10489 (1998)] , *J. Chem. Phys.*, 1999, **110**, 11664–11664.
41 H. Sekino, Y. Maeda, M. Kamiya and K. Hirao, Polarizability and second hyperpolarizability evaluation of long molecules by the density functional theory with long-range correction, *J. Chem. Phys.*, 2007, **126**, 014107.
42 A. Ye, S. Patchkovskii and J. Autschbach, Static and dynamic second hyperpolarizability calculated by time-dependent density functional cubic response theory with local contribution and natural bond orbital analysis, *J. Chem. Phys.*, 2007, **127**, 074104.
43 B. Kirtman, S. Bonness, A. Ramirez-Solis, B. Champagne, H. Matsumoto and H. Sekino, Calculation of electric dipole (hyper)polarizabilities by long-range-correction scheme in density functional theory: A systematic assessment for polydiacetylene and polybutatriene oligomers, *J. Chem. Phys.*, 2008, **128**, 14108.
44 L. E. Johnson, L. R. Dalton and B. H. Robinson, Optimizing calculations of electronic

View Article Online
DOI: 10.1039/D4CP00522H

excitations and relative hyperpolarizabilities of electrooptic chromophores, *Acc. Chem. Res.*, 2014, **47**, 3258–3265.

45 C. Wang, Y. Yuan and X. Tian, Assessment of range-separated exchange functionals and nonempirical functional tuning for calculating the static second hyperpolarizabilities of streptocyanines, *J. Comput. Chem.*, 2017, **38**, 594–600.

46 M. Chołuj, J. Kozłowska and W. Bartkowiak, Benchmarking DFT methods on linear and nonlinear electric properties of spatially confined molecules, *Int. J. Quantum Chem.*, 2018, **118**, e25666.

47 P. Besalú-Sala, S. P. Sitkiewicz, P. Salvador, E. Matito and J. M. Luis, A new tuned range-separated density functional for the accurate calculation of second hyperpolarizabilities, *Phys. Chem. Chem. Phys.*, 2020, **22**, 11871–11880.

48 I. Brandão, T. L. Fonseca, L. R. Franco, H. C. Georg and M. A. Castro, Density functional theory investigation of the second hyperpolarizability of the phenol blue in solution, *Chem. Phys. Lett.*, 2022, **796**, 1–5.

49 K. S. Kaka, P. Beaujean, F. Castet and B. Champagne, A quantum chemical investigation of the second hyperpolarizability of p -nitroaniline, *J. Chem. Phys.*, 2023, **159**, 114104.

50 S. Grimme, M. Steinmetz and M. Korth, How to compute isomerization energies of organic molecules with quantum chemical methods, *J. Org. Chem.*, 2007, **72**, 2118–2126.

51 A. L. Hickey and C. N. Rowley, Benchmarking quantum chemical methods for the calculation of molecular dipole moments and polarizabilities, *J. Phys. Chem. A*, 2014, **118**, 3678–3687.

52 B. Champagne, P. Beaujean, M. de Wergifosse, M. H. Cardenuto, V. Liégeois and F. Castet, Quantum Chemical Methods for Predicting and Interpreting Second-Order Nonlinear Optical Properties: From Small to Extended π-Conjugated Molecules, *Front. Quantum Chem.*, 2018, 117–138.

53 L. Lescos, S. P. Sitkiewicz, P. Beaujean, M. Blanchard-Desce, B. Champagne, E. Matito and F. Castet, Performance of DFT functionals for calculating the second-order nonlinear optical properties of dipolar merocyanines, *Phys. Chem. Chem. Phys.*, 2020, **22**, 16579–16594.

54 D. A. Kleinman, Nonlinear dielectric polarization in optical media, *Phys. Rev.*, 1962, **126**, 1977–1979.

55 V. W. Couling and D. P. Shelton, Hyperpolarizability dispersion measured for (CH3)2O, *J. Chem. Phys.*, 2015, **143**, 1–5.

56 D. V Vlasov, R. A. Garaev, V. V Korobkin and R. V Serov, Measurement of nonlinear polarizability of air, 1979, **2045**, 1033–1036.

57 Y. Shimoji, A. T. Fay, R. S. F. Chang and N. Djeu, Direct measurement of the nonlinear refractive index of air, *J. Opt. Soc. Am. B*, 1989, **6**, 1994.

58 D. M. Pennington, M. A. Henesian and R. W. Hellwarth, Nonlinear index of air at 1.053 μm, *Phys. Rev. A*, 1989, **39**, 3003–3009.

59 D. M. Bishop, Molecular vibrational and rotational motion in static and dynamic electric fields, *Rev. Mod. Phys.*, 1990, **62**, 343–374.

60 L. L. Boyle, A. D. Buckingham, R. L. Disch and D. A. Dromor, Higher polarizability of the helium atom, *J. Chem. Phys.*, 1966, **45**, 1318–1323.

61 R. Tammer, K. Löblein, K. H. Peting and W. Hüttner, Field calibrated measurements of the dc Kerr constants of helium and molecular hydrogen, *Chem. Phys.*, 1992, **168**, 151–158.

62 D. P. Shelton and B. Rugar, The Kerr effect in hydrogen, *Chem. Phys. Lett.*, 1993, **201**, 364–368.

63 R. Tammer and W. Hüttner, The anisotropy of the second hyperpolarizability of molecular hydrogen from the pressure and temperature dependence of the Kerr effect, *Chem. Phys.*, 1990, **146**, 155–163.

64 D. M. Bishop, in *Advances in Chemical Physics*, John Wiley & Sons, Inc., 2007, 1998, vol. 104, pp. 1–40.

65 B. M. Pierce, A theoretical analysis of third-order nonlinear optical properties of linear polyenes and benzene, *J. Chem. Phys.*, 1989, **91**, 791–811.
66 G. R. Meredith, B. Buchalter and C. Hanzlik, Third-order optical susceptibility determination by third harmonic generation. I, *J. Chem. Phys.*, 1983, **78**, 1533–1542.
67 F. Kajzar and J. Messier, Third-harmonic generation in liquids, *Phys. Rev. A*, 1985, **32**, 2352–2363.
68 D. M. Bishop, J. Pipin and M. Rérat, Nonlinear optical properties of H2 and D2, *J. Chem. Phys.*, 1990, **92**, 1902–1908.
69 D. P. Shelton and J. E. Rice, Measurements and calculations of the hyperpolarizabilities of atoms and small molecules in the gas phase, *Chem. Rev.*, 1994, **94**, 3–29.
70 J. S. Ford and D. L. Andrews, Molecular Tensor Analysis of Third-Harmonic Scattering in Liquids, *J. Phys. Chem. A*, 2018, **122**, 563–573.
71 T. Helgaker, P. Jørgensen and J. Olsen, *Molecular Electronic-Structure Theory*, John Wiley \& Sons, Chichester, England, 2000.
72 S. Grimme, Semiempirical hybrid density functional with perturbative second-order correlation, *J. Chem. Phys.*, 2006, **124**, 034108.
73 F. Neese, T. Schwabe and S. Grimme, Analytic derivatives for perturbatively corrected "double hybrid" density functionals: Theory, implementation, and applications, *J. Chem. Phys.*, 2007, **126**, 124115.
74 M. J. Frisch, G. W. Trucks, H. B. Schlegel, G. E. Scuseria, M. A. Robb, J. R. Cheeseman, G. Scalmani, V. Barone, G. A. Petersson, H. Nakatsuji, X. Li, M. Caricato, A. V Marenich, J. Bloino, B. G. Janesko, R. Gomperts, B. Mennucci, H. P. Hratchian, J. V Ortiz, A. F. Izmaylov, J. L. Sonnenberg, D. Williams-Young, F. Ding, F. Lipparini, F. Egidi, J. Goings, B. Peng, A. Petrone, T. Henderson, D. Ranasinghe, V. G. Zakrzewski, J. Gao, N. Rega, G. Zheng, W. Liang, M. Hada, M. Ehara, K. Toyota, R. Fukuda, J. Hasegawa, M. Ishida, T. Nakajima, Y. Honda, O. Kitao, H. Nakai, T. Vreven, K. Throssell, J. A. Montgomery Jr., J. E. Peralta, F. Ogliaro, M. J. Bearpark, J. J. Heyd, E. N. Brothers, K. N. Kudin, V. N. Staroverov, T. A. Keith, R. Kobayashi, J. Normand, K. Raghavachari, A. P. Rendell, J. C. Burant, S. S. Iyengar, J. Tomasi, M. Cossi, J. M. Millam, M. Klene, C. Adamo, R. Cammi, J. W. Ochterski, R. L. Martin, K. Morokuma, O. Farkas, J. B. Foresman and D. J. Fox, 2016, Gaussian 16 Revision A.03;Gaussian, Inc., Wallin.
75 T. Helgaker, S. Coriani, P. Jørgensen, K. Kristensen, J. Olsen and K. Ruud, Recent advances in wave function-based methods of molecular-property calculations, *Chem. Rev.*, 2012, **112**, 543–631.
76 H. D. Cohen and C. C. J. Roothaan, Electric dipole polarizability of atoms by the hartree-fock method. I. Theory for closed-shell systems, *J. Chem. Phys.*, , DOI:10.1063/1.1701512.
77 D. M. Bishop, General dispersion formulas for molecular third-order nonlinear optical properties, *J. Chem. Phys.*, 1989, **90**, 3192–3195.
78 D. M. Bishop and D. W. De Kee, The frequency dependence of nonlinear optical processes, *J. Chem. Phys.*, 1996, **104**, 9876–9887.
79 D. M. Bishop and D. W. De Kee, The frequency dependence of hyperpolarizabilities for noncentrosymmetric molecules, *J. Chem. Phys.*, 1996, **105**, 8247–8249.
80 A. V. Marenich, C. J. Cramer and D. G. Truhlar, Universal Solvation Model Based on Solute Electron Density and on a Continuum Model of the Solvent Defined by the Bulk Dielectric Constant and Atomic Surface Tensions, *J. Phys. Chem. B*, 2009, **113**, 6378–6396.
81 L. F. Richardson and J. A. Gaunt, VIII. The deferred approach to the limit, *Philos. Trans. R. Soc. London. Ser. A*, 1927, **226**, 299–361.
82 M. Medveď, M. Stachová, D. Jacquemin, J. M. André and E. A. Perpète, A generalized Romberg differentiation procedure for calculation of hyperpolarizabilities, *J. Mol. Struct. THEOCHEM*, 2007, **847**, 39–46.
83 A. A. K. Mohammed, P. A. Limacher and B. Champagne, Finding optimal finite field

strengths allowing for a maximum of precision in the calculation of polarizabilities and hyperpolarizabilities, *J. Comput. Chem.*, 2013, **34**, 1497–1507.
View Article Online
DOI: 10.1039/D4CP00522H
84 M. De Wergifosse, V. Liégeois and B. Champagne, Evaluation of the molecular static and dynamic first hyperpolarizabilities, *Int. J. Quantum Chem.*, 2014, **114**, 900–910.
85 J. F. Janak, Proof that ∂E∂ni=ε in density-functional theory, *Phys. Rev. B*, 1978, **18**, 7165–7168.
86 A. Karolewski, L. Kronik and S. Kümmel, Using optimally tuned range separated hybrid functionals in ground-state calculations: Consequences and caveats, *J. Chem. Phys.*, 2013, **138**, 204115.
87 F. Castet, E. Bogdan, A. Plaquet, L. Ducasse, B. Champagne and V. Rodriguez, Reference molecules for nonlinear optics: A joint experimental and theoretical investigation, *J. Chem. Phys.*, 2012, **136**, 024506.
88 V. Postils, Z. Burešová, D. Casanova, B. Champagne, F. Bureš, V. Rodriguez and F. Castet, Second-order nonlinear optical properties of X-shaped pyrazine derivatives, *Phys. Chem. Chem. Phys.*, 2024, **26**, 1709–1721.
89 C. Bosshard, U. Gubler, P. Kaatz, W. Mazerant and U. Meier, Non-phase-matched optical third-harmonic generation in noncentrosymmetric media: Cascaded second-order contributions for the calibration of third-order nonlinearities, *Phys. Rev. B - Condens. Matter Mater. Phys.*, 2000, **61**, 10688–10701.
90 D. S. Elliott and J. F. Ward, Vibrational mode contributions to molecular third order polarizabilities, *Mol. Phys.*, 1984, **51**, 45–63.
91 D. M. Bishop, M. Hasan and B. Kirtman, A simple method for determining approximate static and dynamic vibrational hyperpolarizabilities, *J. Chem. Phys.*, 1995, **103**, 4157–4159.
92 B. Kirtman, B. Champagne and J. M. André, Role of collective modes in vibrational polarizabilities and hyperpolarizabilities of polyacetylene and other quasilinear polymers, *J. Chem. Phys.*, 1996, **104**, 4125–4136.
93 E. A. Perpète, B. Champagne and B. Kirtman, Linear and nonlinear polarizabilities of polydiacetylene and polybutatriene chains: An ab initio coupled Hartree-Fock investigation, *J. Chem. Phys.*, 1997, **107**, 2463–2480.
94 A. P. Persoons, B. M. Van Wonterghem and P. C. Tackx, Measurements of second hyperpolarisabilities of diphenylpolyenes by means of phase-conjugate interferometry, 1991, 220.
95 F. Castet, V. Rodriguez, J. L. Pozzo, L. Ducasse, A. Plaquet and B. Champagne, Design and characterization of molecular nonlinear optical switches, *Acc. Chem. Res.*, 2013, **46**, 2656–2665.
96 F. Castet, C. Tonnelé, L. Muccioli and B. Champagne, Predicting the Second-Order Nonlinear Optical Responses of Organic Materials: The Role of Dynamics, *Acc. Chem. Res.*, 2022, **55**, 3716–3726.